

Titre: Design of millimeter wave self-oscillating mixer with substrate
Title: integrated waveguide technique

Auteur: Jijun Xu
Author:

Date: 2005

Type: Mémoire ou thèse / Dissertation or Thesis

Référence: Xu, J. (2005). Design of millimeter wave self-oscillating mixer with substrate
Citation: integrated waveguide technique [Mémoire de maîtrise, École Polytechnique de
Montréal]. PolyPublie. <https://publications.polymtl.ca/23539/>

 **Document en libre accès dans PolyPublie**
Open Access document in PolyPublie

URL de PolyPublie: <https://publications.polymtl.ca/23539/>
PolyPublie URL:

**Directeurs de
recherche:** Ke Wu
Advisors:

Programme: Non spécifié
Program:

UNIVERSITÉ DE MONTRÉAL

DESIGN OF MILLIMETER WAVE SELF-OSCILLATING MIXER
WITH SUBSTRATE INTEGRATED WAVEGUIDE TECHNIQUE

JIJUN XU
DÉPARTEMENT DE GÉNIE ÉLECTRIQUE
ÉCOLE POLYTECHNIQUE DE MONTRÉAL

MÉMOIRE PRÉSENTÉ EN VUE DE L'OBTENTION
DU DIPLÔME DE MAÎTRISE ÈS SCIENCES APPLIQUÉES
(GÉNIE ÉLECTRIQUE)

JANVIER 2005

© Jijun Xu, 2005

UNIVERSITÉ DE MONTRÉAL

ÉCOLE POLYTECHNIQUE DE MONTRÉAL

Cette thèse intitulée:

DESIGN OF MILLIMETER WAVE SELF-OSCILLATING MIXER
WITH SUBSTRATE INTEGRATED WAVEGUIDE TECHNIQUE

Présentée par: XU Jijun

en vue de l'obtention du diplôme de Maîtrise ès sciences appliquées

a été dûment acceptée par le jury d'examen constitué de :

M. LAURIN Jean-Jacques, Ph.D., président

M. WU Ke, Ph.D., member et directeur de recherche

M. CALOZ Christophe, Ph.D., membre

ACKNOWLEDGEMENTS

I would like to express my gratitude to my supervisor, Professor Ke Wu, for his continuous support, invaluable guidance, and encouragement throughout the work involved in this thesis, which gave me three extremely memorable and fruitful years of studying at École Polytechnique de Montréal.

I would also like to thank each member of our radar group: Jean-Frédéric Gagné, Yanyang Zhao and Hui Zhang. Their knowledge and wisdom have undoubtedly strengthened this work.

I am grateful to Roch Brassard, for his skillful creation and assembly of all the circuits used for this work, and for measuring antennae for me. Sincere thanks also to Steve Dubé and Jules Gauthier, for their advice and creativity; to Jean-Frédéric Gagné and Éric Marsan, for all their help with measurements; and to René Archambault, for managing computer networks.

I appreciate the friendly help provided by Yves Cassivi, Ping Yang, Lin Li, Dominic Deslandes, Feng Xu, Xiaoma Jiang, Xidong Wu, and everyone in Poly-Grames.

Finally, I would like to dedicate the thesis to my husband and my parents. It is their love and support that have enabled me to complete the thesis successfully.

RÉSUMÉ

Dans ce mémoire, la technique du guide d'ondes rectangulaire intégré au substrat (SIW) a été appliquée au design d'un mélangeur auto-oscillant (SOM) en ondes millimétriques. Une structure d'oscillateur à rétroaction a été utilisée dans le design du SOM, et ce dernier a été simulé à l'aide de ADS (Advanced Design System). Un SOM conventionnel a d'abord été construit à l'aide de lignes microruban parallèles couplées pour former un résonateur à rétroaction. Ensuite, un nouveau SOM utilisant la technologie SIW a été conçu et mesuré pour la première fois. Le bruit de phase de ces deux circuits a été mesuré et comparé, et les résultats démontrent que le SOM en technologie SIW procure des niveaux de 10 à 20 dB inférieurs à ceux obtenus avec le SOM en technologie conventionnelle.

Un design amélioré du SOM SIW, basé sur une cavité SIW et sur les principes du SOM en rétroaction, a été présenté. Avec la nouvelle approche, aucun design d'amplificateur n'est nécessaire, et très peu d'ajustement est requis. Ces deux aspects simplifient le design de circuits micro-ondes et rendent le système pratique pour des applications industrielles. Le gain en boucle fermée, réduit par la mauvaise adaptation des ports, a été analysé dans ce nouveau circuit.

Un SOM SIW sous-harmonique, intégré avec une antenne à plaque, a été conçu et mesuré. Le bruit de phase de la fréquence intermédiaire était de -85dBc/Hz @100kHz. La méthode utilisée pour prédire le bruit de phase à la fréquence intermédiaire du SOM SIW à rétroaction fonctionnant à une fréquence plus élevée a été donnée et expliquée par

les résultats de simulation d'une cavité SIW à 28 GHz. La variation de fréquence de l'oscillateur local (LO) causée par les fluctuations du point de polarisation DC du transistor a été testée, et était très faible dans ce design. La perte de conversion de la fonction de mélange sous-harmonique a été mesurée en utilisant une antenne cornet WR28 comme transmetteur et une antenne à plaque isolée comme référence. La perte de conversion moyenne du SOM SIW sous-harmonique était de 8.6 dB, avec une valeur optimale à $V_{ds} = 1.5V$ et $V_{gs} = -0.6V$ en testant la perte de conversion en fonction du point de polarisation DC. Le point de compression à 1 dB de ce récepteur compact était de -9dBm et est causé par le dispositif actif utilisé dans le design.

Ce SOM SIW sous-harmonique intégré avec une antenne à plaque fonctionne comme un récepteur compact et est pratique pour des systèmes de communication en ondes millimétriques qui n'ont pas d'exigences strictes sur la stabilité de la fréquence porteuse. Une nouvelle topologie de SOM SIW fonctionnant comme un élévateur de fréquence a été proposée, et une lentille cylindrique tronquée sur substrat alimentée par des antennes à plaque a été simulée. De plus, une nouvelle structure d'étage d'entrée pour les radars d'imagerie en ondes millimétriques a été présentée. Finalement, une structure de SOM SIW à réflexion a été suggérée comme une avenue de recherche future.

ABSTRACT

In this thesis, the substrate integrated waveguide (SIW) technique was applied in the design of millimeter-wave self-oscillating mixer (SOM). A feedback oscillator structure was used in the SOM design, and the feedback SOM concept was simulated by ADS (Advanced Design System). First, a conventional SOM was built first with a parallel coupled microstrip line as a feedback resonator, and then a novel SIW SOM was designed and measured for the first time. The phase noise performances of these two circuits were measured and compared, which indicates that SIW SOM can provide a phase noise with 10dB to 20 dB less than that of the conventional SOM.

An improved design of SIW SOM, based on the SIW cavity and feedback SOM work principle, is presented. With the new technique, no amplifier design is needed, and almost no tuning is required, which is attractive in microwave circuits design. This technique makes the system very practical in industrial application. The closed loop gain, reduced by port mismatch in the new design, is analyzed.

A subharmonic SIW SOM, integrated with a patch antenna, was designed and measured. Its IF phase noise was $-85\text{dBc/Hz}@100\text{kHz}$. The technique of predicting the IF phases noise of a feedback SIW SOM working at even higher frequency is given, and predicted by the simulation results of a 28GHz SIW cavity. The LO frequency pulled by DC variation was tested, which was very small in this design. The conversion loss of the subharmonic mixing function was measured by using a WR28 horn antenna as transmitter and an isolated patch antenna as reference. The average conversion loss of subharmonic SIW SOM was 8.6dB, and the optimal conversion loss was achieved at

$V_{ds} = 1.5V$, $V_{gs} = -0.6V$ by testing the conversion loss as a function of DC bias. P_{1dB} gain compression of this compact receiver was -9dBm, which was determined by the FET used in the design.

This proposed subharmonic SIW SOM integrated with the patch antenna works as a compact receiver and is practical for millimetre-wave communication system, which requires no strict carrier frequency stability. A number of applications of SIW SOM are suggested for future research. First, a new schematic of SIW SOM working as an up-converter is proposed. Second, a reflect-type SIW SOM structure is suggested by treating SIW cavity as one-port component. Third, a two-dimension substrate lens fed by SIW SOM with integrated patch antenna is simulated and a novel millimetre-wave imaging radar front-end structure is presented.

CONDENSÉ EN FRANÇAIS

DESIGN D'UN MÉLANGEUR AUTO-OSCILLANT EN BANDE MILLIMÉTRIQUE UTILISANT LA TECHNIQUE DU GUIDE D'ONDES RECTANGULAIRE INTÉGRÉ AU SUBSTRAT

L'objectif de ce mémoire est d'étudier et d'implémenter la technique du guide d'ondes rectangulaire intégré au substrat (SIW) dans le design d'un mélangeur auto-oscillant (SOM). Un SIW SOM a été conçu et son bruit de phase comparé à celui d'un SOM conventionnel. Un SIW SOM sous-harmonique à 30 GHz, intégré à une antenne, a été conçu et une recherche a été entreprise afin de déterminer ses performances et de possibles applications dans le domaine des communications en ondes millimétriques.

0.1 Notions théoriques relatives au mélangeur auto-oscillant

Les systèmes de communication conventionnels utilisent deux modules importants et distincts : les oscillateurs et les mélangeurs. L'oscillateur produit un signal stable à la fréquence désirée, et le mélangeur fonctionne comme un convertisseur de fréquence, mélangeant le signal d'entrée avec celui de l'oscillateur. Le besoin de combiner ces deux circuits en un seul, plus compact et plus efficace énergétiquement, a mené au design du mélangeur auto-oscillant (SOM). Un SOM génère lui-même son signal d'oscillateur local. Pour un récepteur, le port radiofréquence (RF) du SOM reçoit un signal qui doit être converti vers le bas en fréquence et le port en fréquence intermédiaire (IF) procure

les produits de mélange désirés. Pour un transmetteur, le port IF reçoit un signal qui est converti vers le haut en fréquence et qui est disponible au port RF. Cette topologie ne permettant pas de satisfaire les critères de performance les plus sévères, des compromis doivent être faits et de nouveaux problèmes doivent être résolus.

Le SOM est issu du design de l'oscillateur verrouillé par injection proposé par Tajima en 1979. L'oscillation et le mélange ont lieu simultanément quand la fréquence du signal injecté est en dehors de la plage de verrouillage en fréquence. Un soin particulier doit être pris dans le design de la boucle de rétroaction pour soutenir les oscillations sans affecter la fréquence IF. Il y a deux topologies de SOM : le SOM à réflexion et le SOM à rétroaction. L'analyse du SOM à réflexion repose sur un modèle de l'oscillateur construit sous la forme d'une résistance négative. Les problèmes posés par ce type de design sont l'injection du signal RF sans affecter le réseau d'adaptation de terminaison, et l'extraction du signal IF sans affecter le réseau de charge. Le SOM à rétroaction est construit en utilisant un amplificateur et un résonateur en cascade, et cette méthode requiert la connaissance du gain en boucle ouverte et le déphasage en fonction de la fréquence. La recherche effectuée dans ce mémoire sur les SIW SOM à rétroaction utilise la topologie d'oscillateur micro-ondes proposée par Cassivi (2003).

0.2 Design du SOM à rétroaction

Le principe du SOM à rétroaction est basé sur la théorie fondamentale des oscillateurs qui repose sur les critères suivants : 1) $G_f = 20\log|S_{21}| > 0\text{dB}$, 2) $\text{Phase} = \text{Arg}(S_{21}) = 0 \text{ deg}$. Ce travail a été simulé avec ADS, en utilisant un modèle

d'amplificateur idéal. La simulation a démontré que lorsque le gain excédentaire de la boucle est grand, l'amplificateur peut couper une partie significative du signal parce qu'il est poussé jusqu'à la saturation. L'onde distordue est riche en contenu spectral, ce qui est nécessaire au design du SOM.

Le transistor ATF36077, de type FET, a été choisi pour la construction de tous les SOM qui seront utilisés dans ce travail. Comme le SOM est un circuit non linéaire, un modèle précis et robuste sous forme de circuit équivalent est requis pour le transistor afin d'obtenir des résultats de simulation qui peuvent être utilisés pour prédire les performances du SOM, comme le bruit de phase et le gain de conversion. Malheureusement, le modèle ADS n'est pas très précis pour ce type de simulation. Cependant, la caractéristique non linéaire du SOM à rétroaction est presque indépendante des conditions de polarisation en DC et le comportement fortement non linéaire du SOM à rétroaction est causé par l'écrêtage. Il en résulte qu'il devient possible d'utiliser un modèle linéaire de FET pour effectuer le design d'un SOM à rétroaction, en mesurant le gain en boucle ouverte du circuit en conditions d'opération linéaire. À l'aide de la technique de calibration TRL, un circuit de test a été conçu pour mesurer les paramètres S du ATF36077 au moyen d'un analyseur de réseau vectoriel et un nouveau modèle a été construit en se basant sur ces résultats de mesure.

Ensuite, un amplificateur à 14 GHz a été conçu, en utilisant le modèle qui vient d'être développé. La similitude entre les résultats simulés et mesurés a confirmé que le modèle était suffisamment précis pour la conception d'amplificateurs linéaires. Des lignes microruban parallèles et couplées ont été utilisées pour fabriquer un résonateur

placé en cascade avec l'amplificateur à 14 GHz afin de fabriquer un SOM simple. L'ensemble du SOM inclut aussi des interrupteurs de calibration, un circuit d'entrée RF, des ports pour le filtre passe-bas (LPF) et la détection de l'oscillateur.

Un SIW SOM a été obtenu en remplaçant les lignes microruban couplées avec une cavité SIW. Une cavité à 14 GHz a été simulée à l'aide de HFSS et réalisée sur un substrat RT5870 ($\epsilon_r = 2.33$, $H=20$ mils). Une machine à construire des prototypes de la compagnie LPKF a été utilisée pour percer des trous d'un diamètre de 31 mils pour réaliser une cavité de 376 x 382 mils. La fréquence de résonance a été estimée à 15.14 GHz au moyen d'une formule, alors que la fréquence de résonance mesurée était de 14.46 GHz. L'écart entre ces résultats est causé par la présence des circuits d'entrée et de sortie sur la cavité. Le facteur de qualité Q de la cavité sans charge est de 540, mais descend à 22.95 lorsqu'il est chargé. Outre la cascade de la cavité et de l'amplificateur qui donne le SOM SIW, toutes les autres composantes du circuit sont inspirées des SOM conventionnels.

L'ajustement du SOM à rétroaction et les mesures ont été effectués dans l'ordre suivant :

- 1) Placer le circuit sous test dans le montage de fixation. Ensuite, procéder à une calibration de type TRL pour déplacer le plan de référence du montage de fixation au circuit.
- 2) L'interrupteur de calibration a été mis en position boucle ouverte pour mesurer le gain et la réponse en phase aux ports d'entrée / sortie du SOM.

- 3) Un ajustement fin avec des stubs microruban a permis de déplacer le déphasage à zéro degré et d'augmenter le gain à plusieurs dB à la fréquence d'oscillation requise.
- 4) L'interrupteur de calibration a été placé en position boucle fermée, le port de détection de l'oscillateur a été branché à l'analyseur de spectre pour vérifier le spectre de l'oscillateur. Si le gain de boucle est suffisamment élevé, la seconde harmonique du spectre sera élevée dans le spectre de sortie.
- 5) Un générateur de signal a été ajouté à l'entrée RF, le port LPF a été raccordé à l'analyseur de spectre pour mesurer la fonction de mélange du circuit.

Ces cinq étapes ont été suivies pour effectuer un ajustement fin des deux circuits SOM. La rétroaction parallèle du SOM oscillait à 14 GHz pendant que le SIW SOM oscillait à 14.2 GHz. Le signal d'entrée RF utilisé avait deux plages de fréquence : (1) 14.1 à 18 GHz, qui se mélange avec la fondamentale du LO ; et (2) 28.2 à 32 GHz, qui se mélange avec la seconde harmonique du LO. Les spectres de mélange testés au port LPF ont été présentés dans ce chapitre.

Le bruit de phase à la fréquence intermédiaire des deux circuits SOM a été mesuré au moyen d'un analyseur de spectre de la compagnie Rohde & Schwartz (FSIQ40). Le décalage en fréquence utilisé allait de 100kHz à 100 MHz. Pour $IF = RF - LO$, le bruit de phase du SOM à rétroaction parallèle était de -60dBc/Hz à 100kHz et celui du SIW SOM était de -80dBc/Hz à 100kHz. Pour $IF = RF - 2LO$, le bruit de phase du SOM était de -60dBc/Hz à 100kHz et celui du SIW SOM était de -75dBc/Hz à 100kHz. En comparant ces valeurs de bruit de phase, il est clair que le SIW SOM offre des niveaux

de 10 à 20 dB inférieurs à ceux obtenus avec le SOM conventionnel. Ceci nous indique que le SIW SOM procure un avantage au niveau du bruit de phase car il requiert un design beaucoup plus méticuleux, en particulier pour la simulation de la cavité, lorsque comparé à un SOM conventionnel.

0.3 Design du SIW SOM sous-harmonique avec antenne à plaque intégrée

Dans ce chapitre, un SIW SOM sous-harmonique avec antenne à plaque intégrée est présenté. Le design combine le circuit SIW SOM présenté au chapitre 2 et l'antenne à plaque conçue au chapitre 3 en un seul circuit planaire, qui fonctionne comme un récepteur avec antenne intégrée. Le coupleur utilisé dans le SIW SOM a été remplacé par l'antenne à plaque à 30 GHz. Le résultat est qu'un signal à 30 GHz reçu par l'antenne peut être démodulé par la 2^e harmonique générée par le LO, résultant en un signal IF à 2 GHz au port LPF. Le SIW SOM sous-harmonique avec antenne intégrée est un circuit simple qui trouve des applications dans les systèmes de communication en ondes millimétriques, dans les transpondeurs, dans les radars d'imagerie ou Doppler, etc.

Le SIW SOM à rétroaction, conçu au chapitre 2, inclut un design d'amplificateur et une boucle de rétroaction construite avec une cavité SIW. La réponse des composantes placées en cascade requiert beaucoup d'ajustement pour bien fonctionner étant donné que l'amplificateur et la cavité SIW ont tous deux des réponses en fréquence abruptes qu'il est difficile de rendre identiques. Un design amélioré, basé sur les caractéristiques de la cavité SIW et sur le principe du SOM à rétroaction, a été proposé. Aucun design d'amplificateur n'est requis, il suffit de cascader la cavité SIW directement avec le

ATF36077. Le résultat est que la réponse du gain est totalement déterminée par la cavité SIW et le déphasage peut être ajusté avec la longueur de la ligne microruban. Avec cette nouvelle approche, les résultats de simulation pour le gain en boucle ouverte et la phase ont démontré une très bonne corrélation avec les résultats mesurés. Ceux-ci ont été obtenus presque sans ajustement, ce qui rend ce design plus pratique dans des applications industrielles. Dans ce type de design, une désadaptation dans la réponse de la cascade en boucle ouverte est inévitable. En supposant que le ATF36077 est unilatéral, la réduction du gain de boucle a été estimée à 2.3 dB dans ce design.

Le bruit de phase à la fréquence IF du SIW SOM sous-harmonique a été mesuré en utilisant le programme conçu à cet effet dans le FSIQ40. Ainsi, le bruit de phase était de -85.7dBc/Hz à 100kHz; -115dBc/Hz à 1MHz et -130dBc/Hz à 10MHz, ce qui est encore mieux que ce qui avait été mesuré au chapitre 2. La formule de Leeson a été appliquée pour prédire le bruit de phase du SIW SOM à des fréquences supérieures. À 28 GHz, la cavité SIW a été simulé avec Ansoft HFSS, et le facteur de qualité Q chargé était de 16. En utilisant la formule de Leeson (qui néglige la contribution prédictive du dispositif sur le bruit de phase et qui compare seulement les facteurs de qualité Q chargé), la valeur du bruit de phase d'un SIW SOM sous-harmonique à 60 GHz a été évaluée à -82dBc/Hz à 100kHz.

Les performances du SIW SOM sous-harmonique intégré avec l'antenne ont été mesurées dans des conditions de laboratoire. La variation de la fréquence d'oscillation causée par les écarts sur la tension de polarisation était très faible dans ce design : avec $V_{ds} = 1.5V$, lorsque V_{gs} est varié de -0.1 à -0.6V, la fréquence de l'oscillateur local passe

de 14.312 GHz à 14.347 GHz, ce qui représente une variation d'environ 35 MHz; avec $V_{gs} = -0.6V$, lorsque V_{ds} est varié de 1.25 à 2V, la fréquence de l'oscillateur local passe de 14.360 GHz à 14.336 GHz, ce qui représente une variation d'environ 24 MHz.

Le montage de test pour le gain de conversion du SIW SOM inclut une antenne-cornet WR28 (MTC), le circuit SIW SOM, une antenne à plaque, un générateur de signaux (SMR40), un wattmètre RF (ML2438A) et une sonde de puissance (MA2474A). L'antenne-cornet fonctionne comme un transmetteur et une mesure de la puissance reçue par l'antenne à plaque est recueillie et utilisée comme référence dans le calcul de la perte de conversion. L'antenne à plaque a ensuite été remplacée par le circuit SIW SOM pour mesurer la puissance du signal IF mélangé. La différence entre la puissance relevée à la sortie de l'antenne à plaque et celle recueillie à la sortie du port IF donne le gain de conversion du SIW SOM. La perte de conversion moyenne du circuit était de 8.5 dB, considérant les pertes du câble.

La sensibilité du gain de conversion à la polarisation de la grille et du drain avec une fréquence RF fixe a été mesurée : Lorsque la tension de grille est réduite de -0.1 à -0.6V, le gain de conversion augmente de 2.2 dB, et le meilleur point d'opération est à $V_{gs} = -0.6V$; avec V_{gs} fixe, lorsque V_{ds} passe de 1.25 à 2V le gain de conversion varie seulement de 1dB. La tension de drain n'affecte donc pas sérieusement le gain de conversion.

Finalement, le point de compression à 1 dB du SIW SOM a été mesuré. Ce test ne peut être effectué efficacement en utilisant le montage précédent, car trop de puissance est alors perdue lors de la transmission. L'alternative a été d'utiliser un signal d'entrée

RF de 18 GHz injecté par le coupleur pour produire un signal IF à 3.653 GHz, et le niveau de ce signal IF a été mesuré sur l'analyseur de spectre tout en variant la puissance du signal d'entrée. La courbe a démontré que le point de compression à 1 dB du SIW SOM était de -9 dBm par rapport à la sortie.

0.4 Travaux futurs

Les SOM ont été surtout utilisés dans les radars Doppler, les transpondeurs, les antennes rétrodirectives, les transmetteurs et les récepteurs de certains systèmes de communication. Ce mémoire propose une structure novatrice pour appliquer le SIW SOM au radar d'imagerie en ondes millimétriques. Le radar d'imagerie réfère aux systèmes et techniques utilisés pour la collecte et le traitement des données en deux dimensions provenant de signaux réfléchis. Habituellement, le système inclut l'antenne, le transmetteur, le récepteur ainsi que les composantes nécessaires au traitement et à l'affichage des signaux. Le design de l'étage d'entrée dans le radar d'imagerie requiert la combinaison optimale des techniques utilisées pour les circuits actifs avec des réseaux d'antennes directives à orientation du faisceau. Les réseaux contrôlés en phase sont couramment utilisés pour l'orientation du faisceau, mais comme la phase entre chaque SIW SOM n'est pas cohérente, il n'est pas facile de procéder au design de ce type d'antenne qui intègre des SIW SOM. Une autre technique de détection électronique est la commutation du faisceau, une solution simple qui consiste à commuter rapidement plusieurs faisceaux fixes. Cette solution s'applique bien à la technique des SIW SOM

puisque les interrupteurs y fonctionnent en fréquence IF, ce qui crée un balayage très rapide et peu dispendieux.

L'antenne lentille sur substrat est aussi une bonne candidate pour l'étage d'entrée des radars d'imagerie en ondes millimétriques utilisant le SIW SOM. Une nouvelle architecture a été décrite et utilise une lentille cylindrique tronquée sur 60° pour former un côté carré et plat qui recouvre l'antenne à plaque d'un réseau de SIW SOM. La lentille cylindrique tronquée permet l'orientation du faisceau. Le signal reçu par l'antenne lentille à des angles spécifiques va être transmis à un élément de l'antenne pour être démodulé par le circuit SIW SOM et produire un signal IF. Des interrupteurs sont placés aux ports IF pour séparer chaque faisceau. Le faisceau étalé ne peut recueillir de l'information qu'en une seule dimension, ce qui n'est pas suffisant pour l'affichage d'images en deux dimensions. Une solution simple à ce problème est de concevoir un transmetteur similaire pour balayer un autre faisceau étalé à la verticale selon une séquence temporelle, en recevant simultanément tous les faisceaux étalés à l'horizontale. Les croisements des deux faisceaux orthogonaux produisent des pixels en deux dimensions.

Le schéma de la structure SIW SOM élévateur de fréquence a aussi été donné : Le signal IF entre par la grille du FET, et le signal RF mélangé émane du drain du FET. Le défi de ce type de circuit repose sur le fait que le signal RF est très près de $2LO$, ce qui implique que l'élévateur de fréquence requiert un filtre en ondes millimétriques avec un facteur de qualité élevé et une réjection élevée à la fréquence de coupure. Un filtre SIW quasi-elliptique est le meilleur choix dans un tel design étant donné que sa topologie,

basée sur les filtres à cavité, démontre d'excellentes performances et qu'il peut être construit sur le même substrat que les autres parties du circuit. Enfin, la structure du SIW SOM à réflexion est suggérée comme avenue de recherche future. Les contributions originales de ce mémoire sont :

- 1) L'analyse et la comparaison du bruit de phase d'un SIW SOM avec un SOM conventionnel.
- 2) Le développement d'une méthode améliorée pour effectuer le design d'un SIW SOM à rétroaction en utilisant un modèle linéaire d'un dispositif actif. Cette méthode peut aussi être appliquée au design d'un oscillateur SIW.
- 3) Un récepteur compact de 30 GHz utilisant un SIW SOM avec une antenne intégrée a été développé et mesuré.
- 4) La proposition d'une nouvelle architecture de l'étage d'entrée d'un radar d'imagerie en ondes millimétriques appliquant la technique du SIW SOM et des antennes lentille sur substrat.

TABLE OF CONTENTS

Acknowledgements.....	iv
Résumé.....	v
Abstract.....	vii
Condensé en Français.....	xi
Table of contents.....	xx
List of figures and tables.....	xxiii
List of abbreviation.....	xxvi
Introduction.....	1
CH 1 Review of the Self-oscillating Mixer.....	4
1.1 Introduction.....	4
1.2 Fundamentals of SOMs.....	5
1.2.1 Reflect-type SOM.....	6
1.2.2 Feedback-type SOM.....	9
CH 2 Feedback SOM Design.....	13
2.1 Feedback SOM Simulation.....	13
2.2 S-Parameter Measurement for ATF36077 and Amplifier Design.....	19

2.3 Feedback SOM Design	21
2.4 SIW Cavity Design	26
2.5 Feedback SIW SOM Design	31
2.6 Comparison of the IF Phase Noise	35
2.7 Summary	40
CH 3 Subharmonic SIW SOM Design with Integrated Patch Antenna	42
3.1 Introduction	42
3.2 Patch Antenna Design	43
3.2.1 Simulation of Patch Antenna	44
3.2.2 Measurement of Patch Antenna	46
3.3 Improved Design of SIW SOM	52
3.4 Mismatch Analysis	57
3.5 Phase Noise Performance of SIW SOM	59
3.6 Electric Performance Measurement	63
3.7 Summary	70
CH 4 Suggestions for Future Work	71
4.1 SIW SOM Applied in an Up-Converter	71
4.2 SIW SOM Applied in Millimetre Wave Imaging Radar	72
4.3 Reflect-type SIW SOM Structure	76

Conclusions..... 78

REFERENCES..... 80

LIST OF FIGURES AND TABLES

Fig.1.1	Conventional transmitter and receiver of communication system	4
Fig.1.2	Communication systems with compact SOM structure.....	5
Fig.1.3	Schematic diagram for one-port negative-resistance oscillators	6
Fig.1.4	Schematic of MMIC SOM.....	7
Fig.1.5	A schematic of the dual-gate FET SOM with active antenna	8
Fig.1.6	Balanced SOM schematic diagram.....	9
Fig.1.7	Feedback oscillator formed by cascade amplifier and resonator.....	10
Fig.1.8	Topology of the SIW feedback oscillator.....	11
Fig.1.9	Two-port feedback SOM diagram	12
Fig.2.1	Open loop gain & phase response vs. frequency	14
Fig.2.2	Simulated spectrum of oscillating frequency	16
Fig.2.3	Waveform clipping simulation of feedback oscillator.....	16
Fig.2.4	Simulated fundamental & harmonic output vs. attenuator	17
Fig.2.5	Mixing signal spectrum of SOM simulation	18
Fig.2.6	RF/IF level & conversion gain as a function of attenuator.....	18
Fig.2.7	Measured and simulated results of the linear amplifier design	20
Fig.2.8	Measured and simulated results of the non-linear amplifier design	21
Fig.2.9	Schematic of parallel CML feedback SOM.....	23
Fig.2.10	Open loop simulation of the conventional SOM	24
Fig.2.11	Layout of parallel CML feedback SOM.....	25

Fig.2.12	Oscillating and mixing spectrum of the conventional SOM	25
Fig.2.13	Rectangular waveguide cavity	26
Fig.2.14	CPW coupling topology with an SIW cavity	27
Fig.2.15	Insertion loss and return loss measurement of SIW cavity.....	28
Fig.2.16	Open loop simulation for SIW SOM.....	32
Fig.2.17	Layout of SIW SOM.....	33
Fig.2.18	Spectrum of RF signal mixing with LO	33
Fig.2.19	Spectrum of RF signal mixing with 2LO	34
Fig.2.20	Experiment setup for measuring the IF phase noise of SOMs	36
Fig.2.21	IF phase noise measurement 1 of the conventional SOM	38
Fig.2.22	IF phase noise measurement 2 of the conventional SOM	38
Fig.2.23	IF phase noise measurement 1 of the SIW SOM.....	39
Fig.2.24	IF phase noise measurement 2 of the SIW SOM.....	39
Fig.2.25	SIW SOM circuit	41
Fig.3.1	Simulation results of patch antenna without the affection of feed	45
Fig.3.2	Patch antenna with inset microstrip feed	46
Fig.3.3	Experimental setup for measuring input impedance	47
Fig.3.4	S-parameter measurement of patch antenna	47
Fig.3.5	Test setup for antenna parameters measurement	48
Fig.3.6	Simulated and measured pattern of principle planes	50
Fig.3.7	Measured frequency response of E plane pattern	51
Fig.3.8	Measured frequency response of H plane pattern.....	51

Fig.3.9	Measured S21 of the amplifier and the SIW cavity.....	52
Fig.3.10	Simulated and measured open loop response of ATF36077 cascaded with SIW Cavity	54
Fig.3.11	Layout of SH SIW SOM integrated with patch antenna	55
Fig.3.12	SH SIW SOM integrated with patch antenna circuit.....	55
Fig.3.13	Mixing spectrum of SH SIW SOM	56
Fig.3.14	Measured IF phase noise of SH SIW SOM.....	56
Fig.3.15	Input and output reflection of SH SIW SOM.....	59
Fig.3.16	Oscillator SSB phase noise as a function of offset frequency to carrier	60
Fig.3.17	Simulated results of a 28GHz SIW cavity.....	63
Fig.3.18	Measured oscillating frequencies drift as a function DC bias	64
Fig.3.19	Conversion gain test setup of SIW SOM integrated with patch antenna	67
Fig.3.20	Measured conversion loss as a function of the V_{ds} and V_{gs}	68
Fig.3.21	P_{1dB} gain compression measured Result	69
Fig.4.1	Schematic of an SIW SOM up-converter	72
Fig.4.2	Front-end structure of SH SIW SOM integrated with cutoff cylinder lens	74
Fig.4.3	Simulated beam scan of cylinder lens fed by four patch elements.....	75
Fig.4.4	The working of two-dimension imaging construed by fan beam steering ..	76
Fig.4.5	Layout of reflect-type SIW SOM	77
Table 2.1	Comparison of IF phase noise for SOM and SIW SOM	37
Table 3.1	Tested data of conversion loss	66

LIST OF ABBREVIATION

SOM	Self-Oscillating Mixer
SIW	Substrate Integrated Waveguide
RF	Radio Frequency
IF	Intermediate Frequency
SH	Sub-Harmonic
DC	Direct Current
BPF	Band-pass Filter
LPF	Low-pass Filter
FET	Field Effects Transistor
LO	Local Oscillator
MMIC	Monolithic Microwave Integrated Circuit
LMDS	Local Multipoint Distribution Services
ADS	Advanced Design System
MoM	Method of Moments
SSB	Single Side Band
ILO	Injection-locked Oscillator

INTRODUCTION

Imaging technologies using millimetre-wave offer unique measurement means in many application areas, such as aircraft landing sensor, plasma diagnostics, ocean remote sensing, autonomous landing guidance and train tracking and control. Imaging radar refers to systems and techniques for collecting and processing radar backscatter data from a planar array. Antenna arrays in imaging systems act as spatial collector to distinguish each pixel in the field of view. One kind of compact front-end design of imaging radar is frequency-conversion-type active integrated antenna (AIA) with circuits generating the LO internally using self-oscillating mixer (SOM). For millimeter-wave applications and circuit simplicity, subharmonic SOM is chosen in many designs.

The objective of this thesis is to investigate and implement a new SOM structure for millimetre-wave imaging radar. Recently, a new scheme called substrate integrated waveguide (SIW) has been presented and developed as an attractive technique for low-loss, low-cost, and high-density integration millimetre-wave components. A novel feedback SOM by using a SIW cavity as resonator is presented in this thesis and the circuit is called as SIW SOM. Because the SIW cavity is used to stabilize the oscillating frequency, an improved IF phase noise is obtained, which allows the possibility to design a planar integrated front-end for millimetre-wave communications. A simple technique, according to characteristics of the SIW cavity and the feedback SOM working principle, is proposed to design a SIW SOM. A 30GHz subharmonic SIW SOM with integrated patch antenna is complemented and its electrical performance is measured and analyzed.

Chapter 1 reviews the different structure design of the SOM. The main advantages of the SOMs are low power consumption, low cost, and reduced chip size and weight, which can profoundly impact the performance of the front-end transceiver circuits. The challenge of the SOM design is that not only it requires accurate large-signal model of active device, but needs appropriate circuits simulation software. However, development of large-signal transistor model is a very time consuming progress. In this thesis, the loop-gain measurement technique [8] is used for the SOM design, based on small signal S-parameters of the transistor.

The active device used in the thesis is AFT36077, a low noise pHEMT transistor from Agilent. At the beginning of Chapter 2, a linear model of the AFT36077 is built after the S-parameter testing is completed on it. A conventional feedback SOM is designed by cascading an amplifier and a parallel coupled microstrip line. Afterward, a novel SIW SOM design is discussed in detail. Since the resonator circuit—SIW cavity is an important part of the oscillator circuit, its design, simulation, and measurement are presented in a separated section. Two SOM structures are compared for their mixed IF phase noise, to highlight the advantage of SIW SOM.

In Chapter 3, a subharmonic self-oscillating mixer, integrated with the patch antenna is designed and measured. The completed design makes this subharmonic SOM work as a compact receiver. A simple design technique is proposed, which means that no amplifier design is needed and the phase noise is only determined by the cavity. Therefore, the IF phase noise of the newly designed circuit is improved compared with the design in Chapter 2. Port mismatch is discussed in the new design, and Leeson's

formula is applied to predict the phase noise performance of the SIW SOM working at even higher frequency. At the end of this chapter, the working performances, such as the oscillating frequency shift as a function of DC bias, the conversion gain of the subharmonic SIW SOM, the optimal DC bias to achieve the best conversion gain, and the gain compression of the SIW SOM, will be measured and discussed.

Chapter 4 presents an up-converter application of SIW SOM. A new millimetre-wave imaging radar front-end structure is proposed, where the SIW SOM with integrated patch antenna servers as feed to a substrate lens. A reflect-type SIW SOM structure is also proposed for future research in this area.

CHAPTER 1

REVIEW OF SELF-OSCILLATING MIXER

1.1. Introduction

Conventional communication systems make use of two important but separated modules known as oscillators and mixers. As shown in Fig.1.1, the oscillator produces a stable signal at the desired frequency and the mixer works as frequency converter by mixing the input signal with the oscillator signal. The need for combining the two circuits into one that is more compact and consumes a lower power gives rise to the design of self-oscillating mixers (SOM). As shown in Fig.1.2, SOM generates internally the local oscillator signal that makes the circuit time varying. As for the structure with radio frequency (RF) down converted to intermediate frequency (IF) is applied in a receiver; and for IF input signal up converted to RF is used in transmitter.

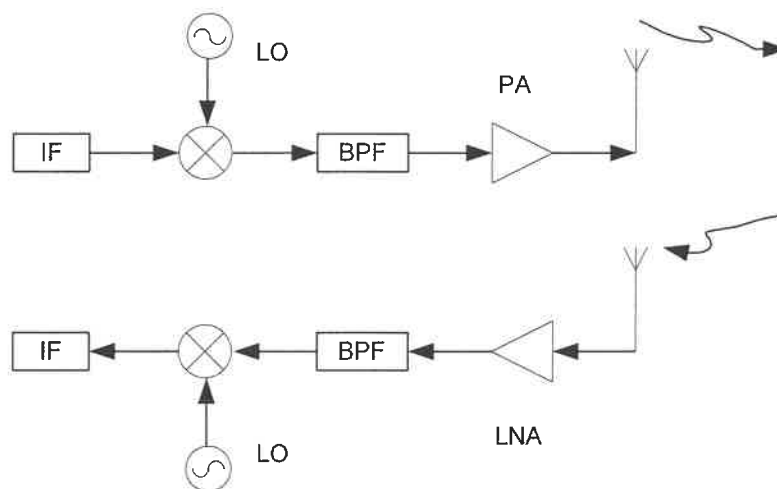


Fig.1.1 Conventional transmitter and receiver of communication system

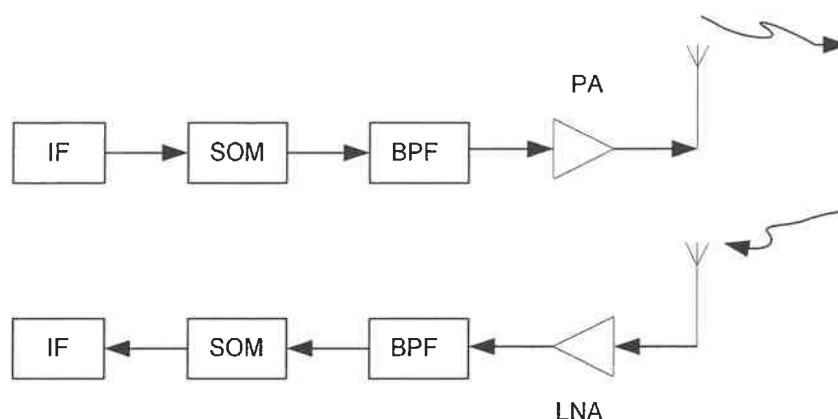


Fig.1.2 Communication systems with compact SOM structure

1.2. Fundamentals of SOMs

The self-oscillating mixer concept first came from an injection-locked oscillator (ILO) proposed by Tajima in 1979 [1]. Tajima described a transmission-type ILO by injecting a reference signal into the gate, while the output power of oscillator was obtained at the drain. Oscillators with separated signal port and output power port also work as self-oscillating mixers when they satisfy two basic conditions:

1. a feedback loop must be designed to provide enough gain to make the transistor work into its non-linear range, but still be effective enough to sustain oscillation;
2. the frequency of injecting reference signal must be out of the locking range.

As the SOM derived from ILO, the two types of SOM structure are the same as oscillator types: reflect-type SOM (Sec.1.2.1) and feedback type SOM (Sec.1.2.2). Each corresponds to a different analysis method.

1.2.1. Reflect-type SOM

Reflect-type SOMs are based on modeling of the oscillator as a negative resistance. The key problems of reflect-type SOMs design are how to inject RF signal without affect the terminating network, and also how to extract the IF mixing frequency without affect the load network. Negative-resistance oscillators' general schematic, oscillation and stability conditions are shown in Fig.1.3, [2].

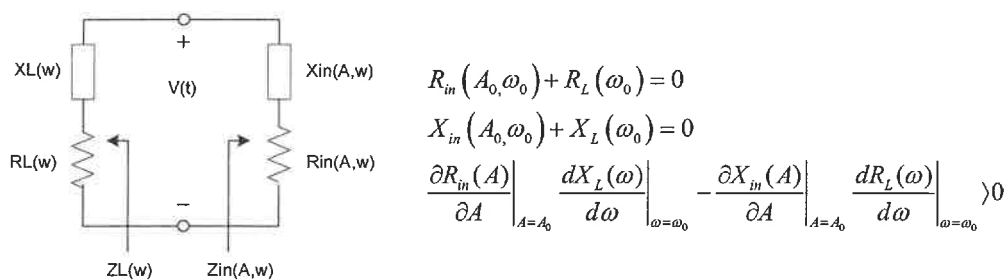


Fig.1.3 Schematic diagram for one-port negative-resistance oscillators

The SOM designs proposed in [3], [4], [5] and [6] are all based on reflect-type oscillator analysis. A 77GHz subharmonic MMIC SOM corresponding to the schematic shown in Fig.1.4, was described in [5]. The aim of source feedback is to present a short circuit to the source of the device at RF and simultaneously provide feedback at the LO frequency. The reactive gate feedback is usually realized by using an open circuit stub, which could not be used in this case, since the RF needs to be injected at the gate. A BPF is placed between the gate and the RF port to isolate the LO from the RF. At LO frequency, the filter presents as a capacitive reactance which can be transformed to the

desired gate feedback reactance by adding a 50Ω transmission line of the adequate length between the gate and the RF filter. This MMIC SOM is designed with one transistor, so two networks should be connected to the gate, one is a terminating network designed for the oscillator circuit, and the other is an RF input network for mixer function. However with a single active device, integration of an antenna and good performance are not easy to achieve.

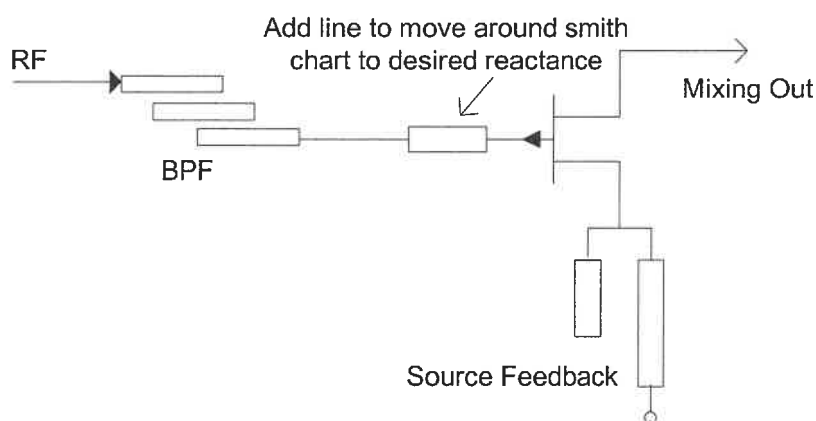


Fig.1.4 Schematic of MMIC SOM

An alternative choice is to use dual-gate FET, the antenna is connected to one gate of the FET while the oscillator is formed at the other gate of the FET. A C-band SOM integrated with an active antenna to the schematic shown in Fig.1.5, was designed in [6]. The advantage of such a configuration is that except for conversion gain, the circuit presents an intrinsic separation of the RF signal port from the termination port of local oscillator, when a direct combination of the corresponding powers is made inside the

device. This avoids the use of cumbersome passive couplers and consequently reduces the number of components.

A more attractive design is a balanced self-oscillating mixer described in [3] and [4]. The balanced SOM proposed in [4] served as an up-converter which overcame the disadvantage of poor LO to RF isolation when a single SOM used in the design. In addition, the work in [3] took advantage of the symmetric characteristics of balanced SOM to combine it with the modal radiation characteristics of quasi-Yagi antenna. This balanced approach enhances the generation of the second harmonic. The general balanced SOM structure is described in Fig.1.6.

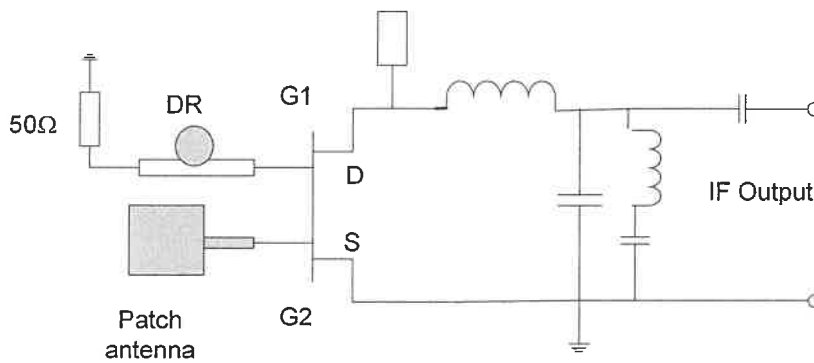


Fig.1.5 A schematic of the dual-gate FET SOM with active antenna

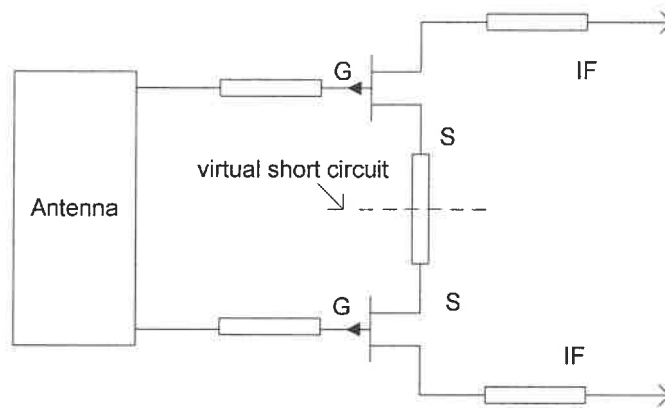


Fig.1.6 Balanced SOM schematic diagram

The optimum conversion gain of reflect-type SOM can be achieved by adjusting the DC bias of the gate and drain. The sensitivity of the conversion loss described in [3], with reference to the gate and drain bias voltage, indicated that the conversion efficiency was optimum within a gate voltage window, and that the conversion loss was saturated with a drain bias higher than a specified value.

1.2.2. Feedback type SOM

Feedback oscillator method [7] involves open-loop gain and phase response versus frequency. Consider the amplifier-resonator cascade in Fig.1.7, the forward gain at a given frequency is

$$G_f = 20 \log |S_{21}| \quad (1.1)$$

$$Phase = \arg(S_{21}) \quad (1.2)$$

where S_{21} is the magnitude of the forward-scattering parameter for the cascade at a given frequency. Oscillation occurs at the frequency of a zero-degreed phase shift and higher than zero-dB open-loop gains. The phase shift of an amplifier-resonator cascade becomes difficult to manage at microwave frequencies, but recently the work in [8] proposed an easy way to design a 6 GHz feedback oscillator using small signal S-parameter measurement. The open loop-gain measurement allows the tuning of the oscillator while operating in a linear mode, and shows the effect of the bias network and the out-of-band response.

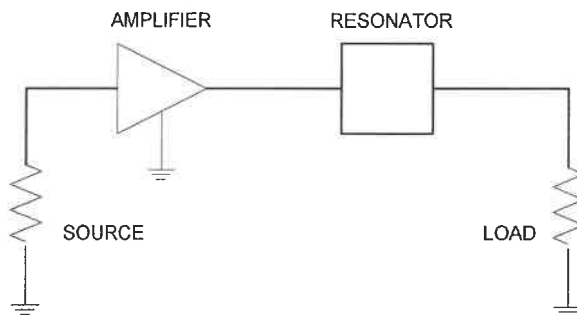


Fig.1.7 Feedback oscillator formed by cascade amplifier and resonator

Cassivi first proposed a novel low-cost microwave oscillator topology in [9], and a 12GHz feedback oscillator was designed and constructed. This new feedback oscillator has developed a substrate integrated waveguide cavity in the design. The schematic of the novel SIW oscillator is illustrated in Fig.1.8. Of the three current probes, one served as an output port while another coupled power to the positive feedback loop.

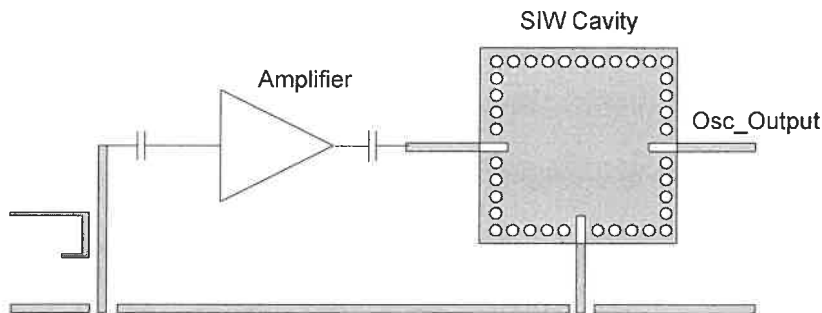


Fig.1.8 Topology of the SIW feedback oscillator

Related to feedback oscillator design, the feedback SOM function can be achieved by connecting the RF signal to the oscillator input port (the gate of FET). Then sum and difference products are generated when the RF signal mixes with the internally generated oscillation. Unlike reflect-type SOM, whose conversion efficiency depends on DC bias voltage, the highly nonlinear condition of feedback oscillators depends on heavy clipping in the active device. Rhea suggested in [7] that clipping occurs when the transistor is driven into saturation and/or cutoff during a portion of the waveform cycle. If the excess loop gain is small, waveforms are nearly sinusoidal and quasi-class-A operation conditions exist. If the excess loop gain is large, the active device may remain saturated or cut off over a significant portion of the waveform period. This results in class-C operation conditions, which are normally undesirable in the design of high-efficiency, high-output power oscillators, but exactly required performance in the feedback SOM design. The schematic of a feedback SOM structure is illustrated in Fig.1.9.

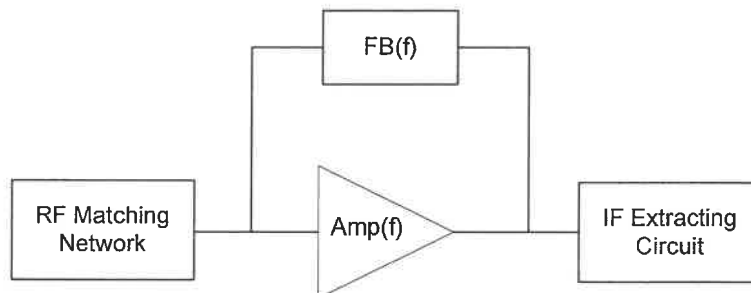


Fig.1.9 Two-port feedback SOM diagram

Design, analysis and application of the feedback SOMs were proposed in [10], [11], [12]. The authors of [10] and [12] have constructed the SOM with a dielectric resonator (DR) stabilization, and a new balanced SOM up-converter with integrated antenna was presented in [11].

Compared with reflect-type SOM, the feedback SOM has the advantage of adding an RF signal input circuit and an IF extracting circuit has less effect on working state of the oscillator. The conversion efficiency of feedback SOM is almost independent of the DC bias of transistors, which is predominantly determined by the open loop gain. Though a large-signal analysis can give accurate design of the feedback SOM as shown in [10], a good design can also be achieved through small signal S-parameters measurement and fine tuning, as shown in [11].

CHAPTER 2

FEEDBACK SOM DESIGN

2.1 Feedback SOM Simulation

The principle of the feedback SOM design is based on the feedback oscillator fundamentals described in [7]. Feedback oscillators are constructed with an amplifier and a resonator in cascade. To facilitate the analysis, the cascaded circuit is treated as a two port network rather than a one port network by breaking the feedback loop. The oscillation criteria, which in the open-loop involve gain and phase response versus frequency, are described as follows:

- 1) $G_f = 20 \log |S_{21}| > 0 \text{ dB}$,
- 2) $Phase = Arg(S_{21}) = 0 \text{ deg}$.

Assuming that the oscillation criteria are satisfied, an oscillator is realized by connecting the feedback loop. Oscillations then build up until the excess loop gain is lost because of clipping in the active device. Clipping occurs when the transistor is driven into saturation and cut off during a period of the signal cycle. If the excess loop gain is small, waveforms are nearly sinusoidal where a quasi-class-A operation conditions exist. If the excess loop gain is large, the active device may remain saturated, and the waveform cuts off over a signal period, which is in class-C operation condition. The class-C operation condition is normally undesirable in the design of high-efficiency, high-output power oscillators. In contrast, it is well suited to our feedback SOM design, because in this case, the active device is driven into saturation that makes the mixer function available.

Ideal ADS models are used to simulate the feedback SOM working principle, and to evaluate how, in the active device, clipping produces mixing functions of the feedback oscillator. The simulation schematic of the feedback SOM includes three functional circuits: oscillation circuit, RF input circuit and IF extraction circuit. The oscillator is constructed by models of an amplifier, a resonator and an attenuator. The amplifier is set as 8 dB gain and 5 dBm output P_{1dB} ; the resonator is realized by a Chebyshev filter; and the attenuator is an ideal model in ADS. An S-parameter simulator is used to obtain the open loop gain and phase response as a function of frequency. The simulated results are shown in Fig.2.1 and the expected oscillating frequency is about 14 GHz, since at this frequency the loop gain is 7.7 dB and the phase shift is -3.7 deg, which satisfies the oscillation criteria.

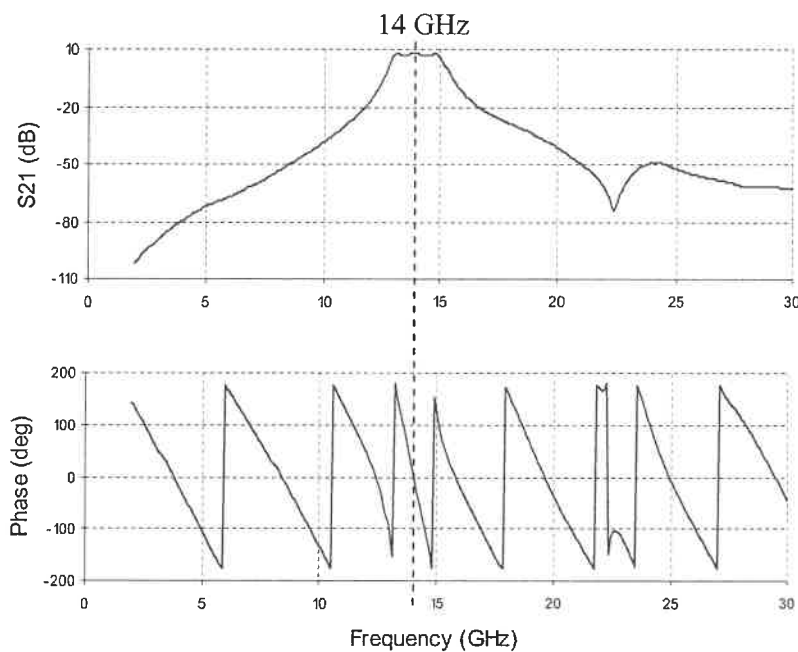


Fig.2.1 Open loop gain & phase response vs. frequency

The closed loop response is simulated by harmonic balance and the Oscport simulator in ADS [16]. The spectrum at the output of the oscillator, with attenuation level at 7 dB, is displayed in Fig.2.2. The fundamental oscillation frequency is 14.03 GHz, which is very close to the open-loop S-parameter simulated results given in Fig.2.1. Changing the attenuator level in the circuit could change the strength of feedback. Strong feedbacks should drive the amplifier into saturation and clipped or distorted a sinusoidal waveform. A simulation of this phenomenon is shown in Fig.2.3. When the attenuator level is 7 dB, the whole system loop gain is only 1dB ($G_{loop} = G_{amp} - G_{atten} = 8dB - 7dB = 1dB$). Such a small loop gain makes a linear oscillator, so the waveform is a sinusoidal signal. When the attenuator is changed to 3 dB, the loop gain increases to 5 dB ($G_{loop} = G_{amp} - G_{atten} = 8dB - 3dB = 5dB$). In this case, the sinusoidal waveform is distorted, because of the amplifier saturation. The distorted waveform includes detailed frequency information, which is required in the mixing function of the SOM design. The simulated fundamental and harmonic levels of the oscillator as a function of the attenuator are shown in Fig.2.4. With the attenuator level increased from 0 dB to 7 dB, the fundamental level is decreased by just several dB, while the harmonic level is quickly decreased from 0 dBm to -22 dBm. That leads to the conclusion that the loop gain affects the harmonic level more than its fundamental part.

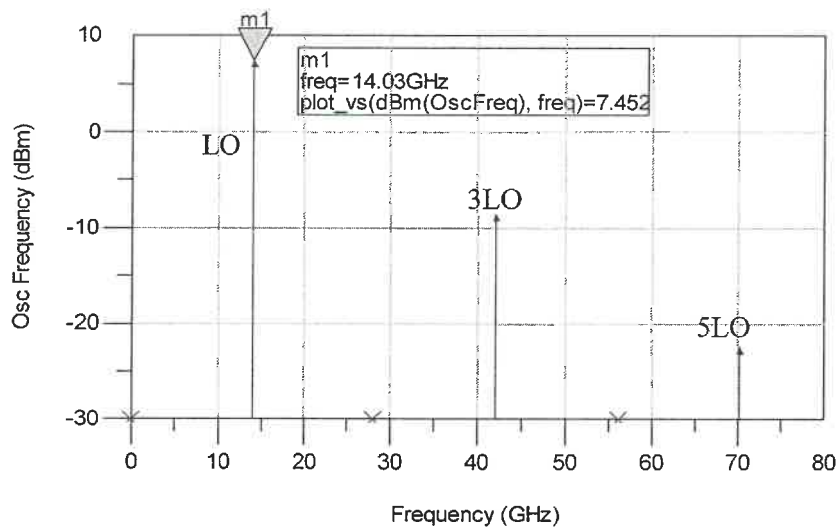


Fig.2.2 Simulated spectrum of oscillating frequency with attenuation level at 7 dB

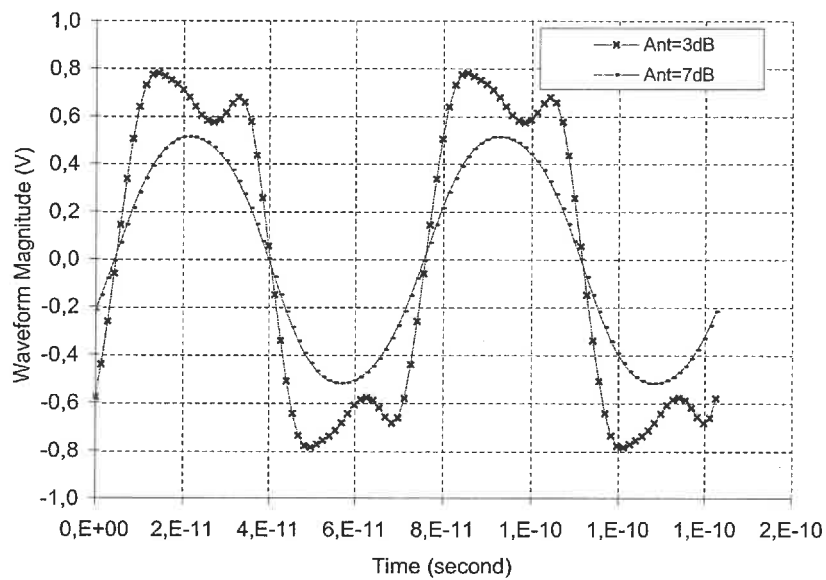


Fig.2.3 Waveform clipping simulation of feedback oscillator

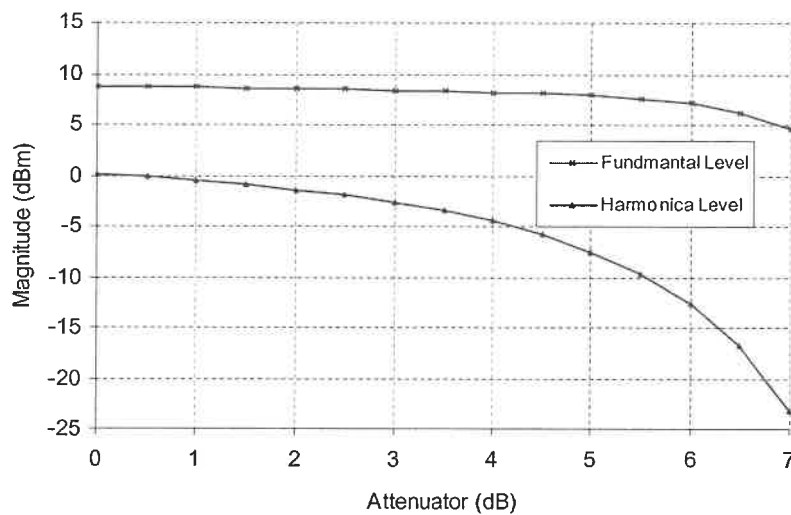


Fig.2.4 Simulated fundamental & harmonic output vs. attenuator

The mixing function is simulated by adding a 30 GHz RF signal with -20 dBm level from RF input circuit. The simulated mixing spectrum at the output of the IF extraction circuit is shown in Fig.2.5. The level of IF signal and RF signal, and the conversion gain, which is equal to the IF level minus the RF level, as a function of the attenuator are all plotted in Fig.2.6, with the attenuator level sweeping from 0 dB to 7 dB. When the attenuator is set at 0 dB to 5 dB, the conversion gain of this feedback SOM is almost -5 dB; once the attenuator is increased to 7 dB, the simulated conversion gain quickly drops to -12 dB. That means a small loop gain also lowers the mixing signal level and the conversion gain of SOM.

The simulated results of the oscillation harmonic level, as well as the IF power and conversion gain as a function of the loop gain, indicates that in feedback SOM structure,

if want oscillator and mixer works simultaneously with good conversion efficiency, the circuit should be designed with a sufficient loop gain.

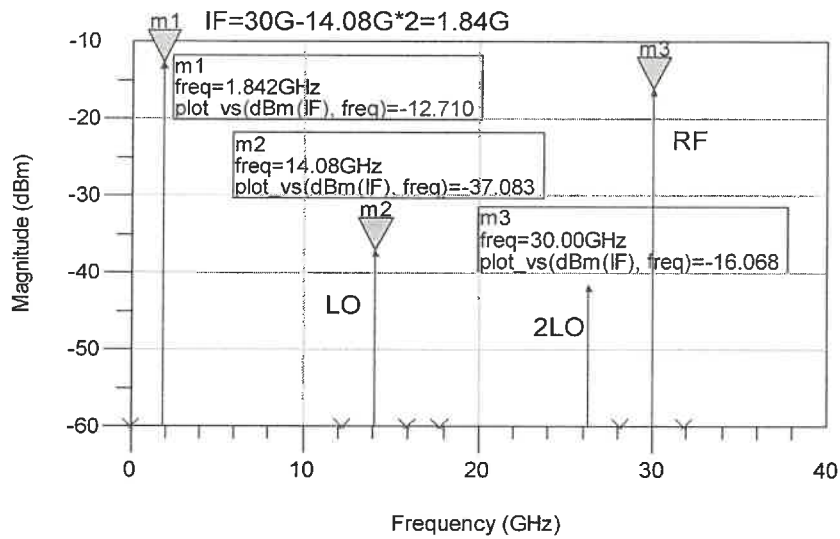


Fig.2.5 Mixing signal spectrum of SOM simulation

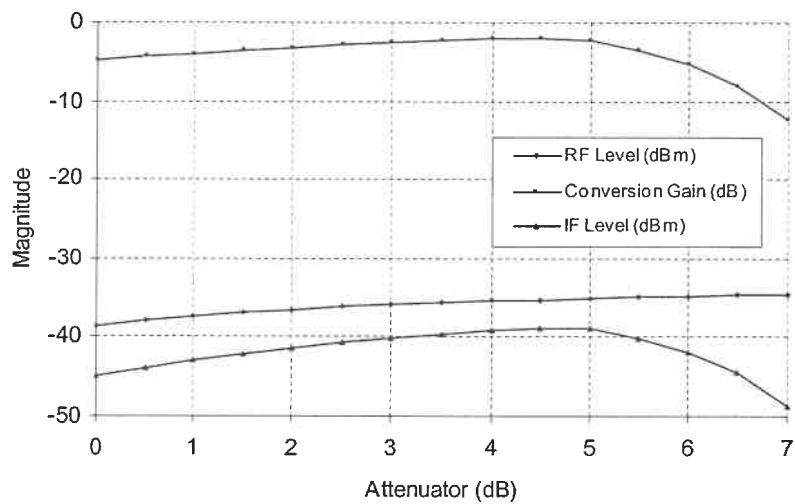


Fig.2.6 RF/IF level & conversion gain as a function of attenuator

2.2 S-Parameter Measurement of the ATF36077 and Amplifier Design

A low noise pHEMT transistor ATF36077 from Agilent was chosen to design the circuits in this thesis. Though Agilent provides a model of ATF36077 in its ADS components library, it is not quite accurate for practical design. The measured results of the amplifiers and oscillators designed on that model turn out to be quite different from the simulated results. In a feedback SOM design, both amplitude and phase response are very sensitive to circuit working, so it is necessary to measure the S-parameters of the transistor in our lab fabrication conditions. A testing circuit was made with TRL calibration technique to test the S-parameter of the ATF36077 by a network analyzer. Several measurements are done at different values of DC bias. The measured results differ greatly from the simulated results that are obtained from the ADS model. To solve the problem, a new model of the ATF36077 built, based on the measured S-parameters including the effects of the DC bias network. The built model used as a component in ADS to design amplifiers and SOM circuits. Two kinds of amplifiers, with different DC bias, designed with the built model to verify if the model work well. A linear amplifier biased at $V_{ds} = 1.5V$, $V_{gs} = -0.21V$, $I_{ds} = 10mA$, and a nonlinear amplifier biased at $V_{ds} = 1.5V$, $V_{gs} = -0.46V$, $I_{ds} = 1mA$. Simulated and measured results of these two amplifiers are presented as follow:

- 1) $V_{ds} = 1.5V$, $V_{gs} = -0.21V$, $I_{ds} = 10mA$

A linear 14GHz amplifier is designed at this DC bias. The simulated results based on the new model and the measured results of the constructed circuit are shown in Fig.2.7. The

simulated results are in very good match with the measured results, which means a good reliability of the new model at this linear DC bias condition.

$$V_{ds} = 1.5V, V_{gs} = -0.21V, I_{ds} = 10mA$$

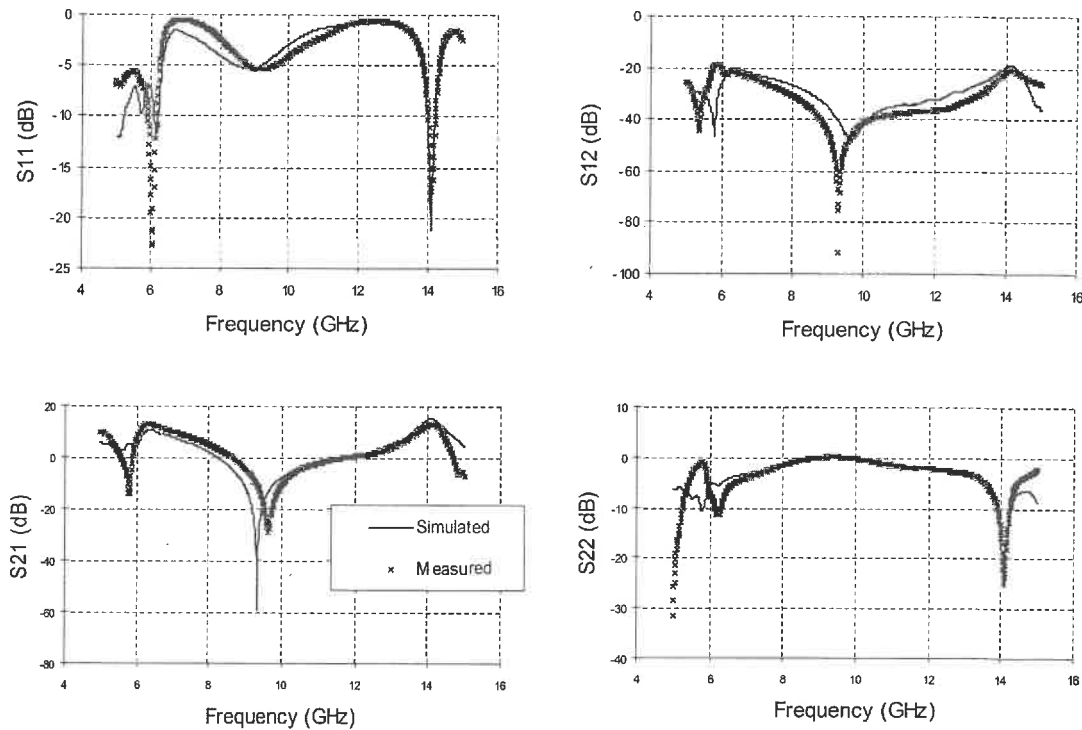


Fig.2.7 Measured and simulated results of the linear amplifier design

$$2) V_{ds} = 1.5V, V_{gs} = -0.46V, I_{ds} = 1mA$$

Another 14 GHz amplifier biased at this DC condition designed; the simulated and the measured results are shown in Fig.2.8. It is clear that the measured results are not close to the simulated results. This is because at this DC bias condition, the ATF36077 is working in a non-linearity region, and a good model performance cannot be achieved

only with an S-parameter test. So, the S-parameter test is suitable only for building a linear model of the transistor, and it doesn't work well at the nonlinear condition.

$$V_{ds} = 1.5V, V_{gs} = -0.46V, I_{ds} = 1mA$$

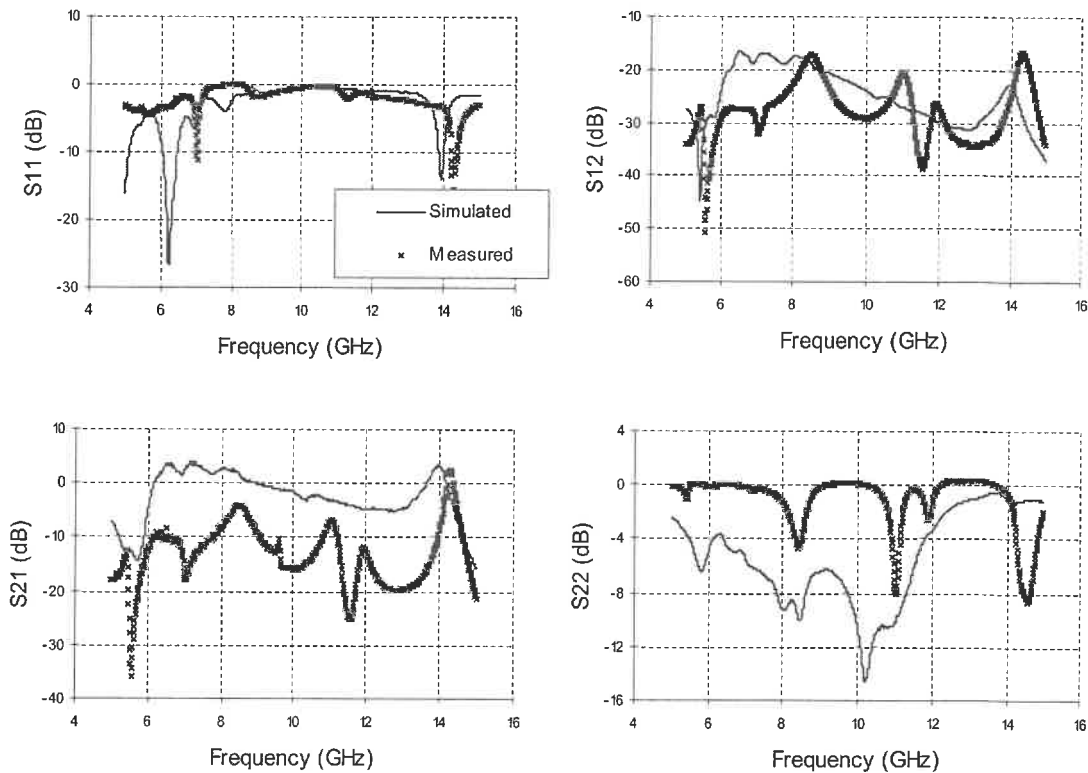


Fig.2.8 Measured and simulated results of the non-linear amplifier design

2.3 Feedback SOM Design

The self-oscillating mixer is a typical nonlinear circuit. It is necessary to build a large signal model of FET, in order to predict accurately the SOM's performance in phase noise, conversion gain, noise figure, etc. Development of an equivalent circuit model is,

however, a very time consuming process. Instead of using the large-signal model of the ATF36077, the model used in this work is a linear one built on S-parameter measurement. As last section indicated, the linear model built on small signal measurement is accurate in linear circuit design, but doesn't work well in nonlinear circuit design. So the question is how to use the linear model to design our highly nonlinear SOM. Fortunately, as stated in Section 1.2.2 of Chapter 1, the feedback SOM's nonlinear performance is almost independent of the DC bias condition, and the highly nonlinear operation of a feedback SOM comes from heavy clipping of active device with a large excess loop gain. As a result, it is reasonable and practical to design the feedback SOM circuits by using a linear transistor model. However, predicting the performance of feedback SOM is still difficult based on linear model simulations. Therefore, many experiments are required in this work to search for the basic properties of feedback SOM.

A conventional SOM built by cascading an amplifier with a parallel coupled microstrip line (CML) and its schematic is shown in Fig.2.9. The amplifier is designed as conjugate match at the input and output of the ATF36077. The parallel CML is designed at a center frequency of 14.3 GHz. Since the simulated results of the CML obtained by the ADS circuit model and by ADS-MoM are quite close, we can use the circuit model to do simulation for the whole SOM design. The simulated open loop gain and phase responses vs. frequency of the design are shown in Fig.2.10, and the results demonstrates that the oscillator would occur at around 13.85 GHz. Attempts to use a harmonic balanced simulation to test the closed-loop response of the circuit failed to

converge. However, the S-parameter and harmonic balanced simulations performed in Section 2.1 showed that the open-loop S-parameter simulation is quite close to the closed-loop harmonic balanced simulation. So we can use the open loop simulated results to predict the oscillating frequency, which is 13.8 GHz in this design.

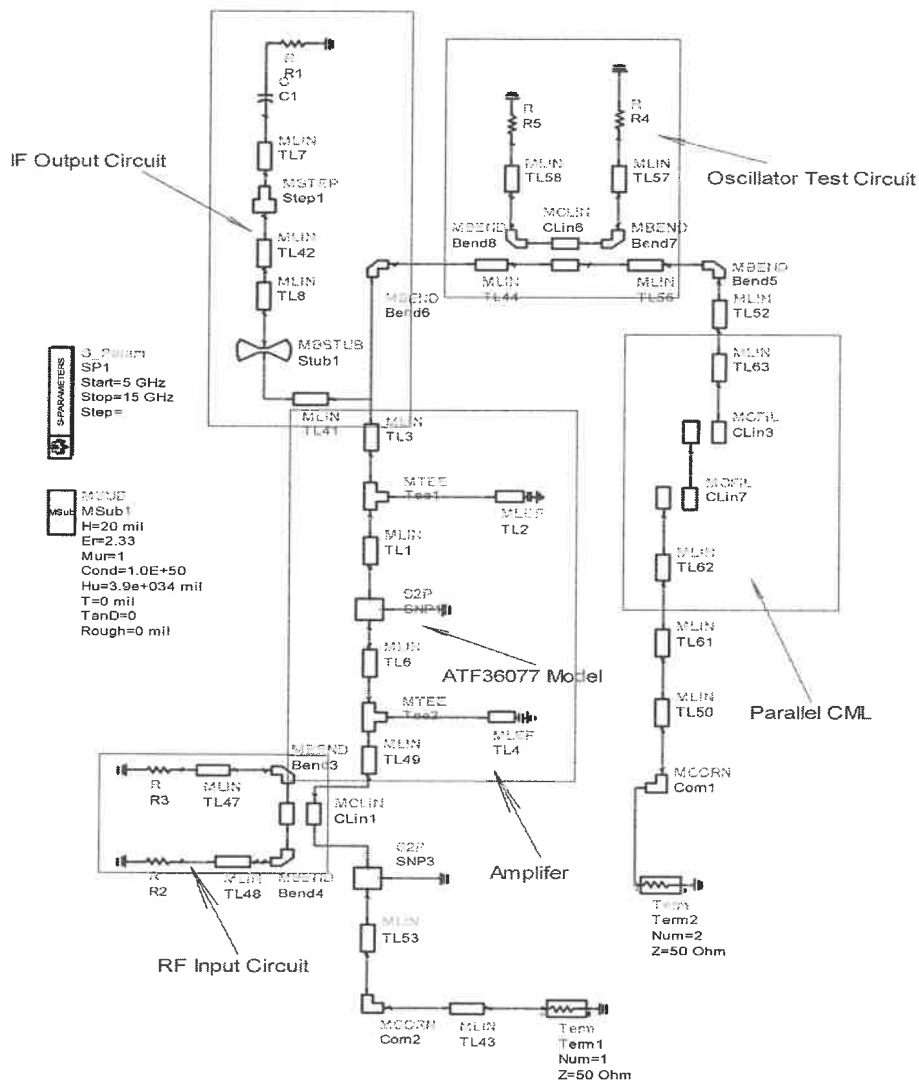


Fig.2.9 Schematic of parallel CML feedback SOM

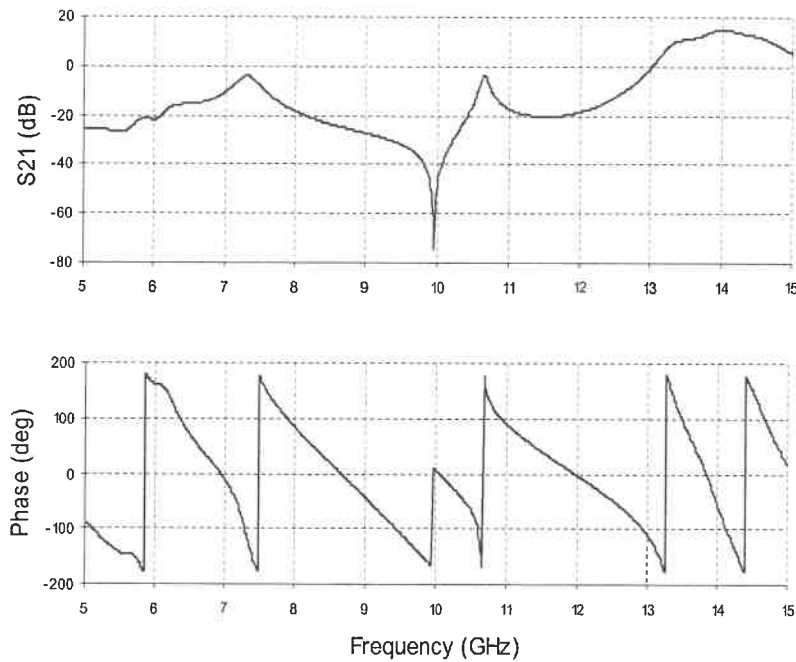


Fig.2.10 Open loop simulation of the conventional SOM

The layout of the parallel CML feedback SOM is shown in Fig.2.11. It includes five ports: *P1*, *P2*, *RF Input*, *IF Output*, *Oscillator Detect*, and two calibration jumpers. The lengths of *L1*, *L2* and *L* are related by the following equation:

$$L = L1 + L2 - 2l_{cal} \quad (2.1)$$

where

l_{cal} depends on the length of TRL calibration kit lines. The testing reference plane can be specified by using TRL calibration technology.

The oscillating and mixing spectrums are shown in Fig.2.12. The level difference of 2LO and LO is 6.3 dB, which means the saturation of the FET is strong and the mixing

function would work well. The oscillating frequency is 14.4 GHz, higher than the simulation results.

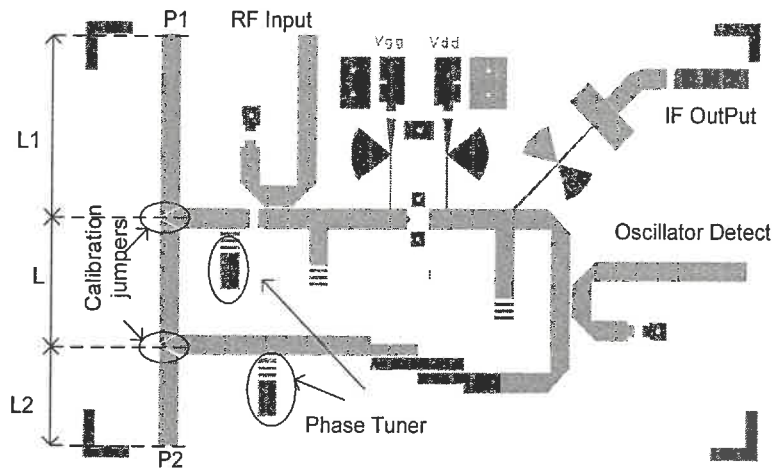


Fig.2.11 Layout of parallel CML feedback SOM

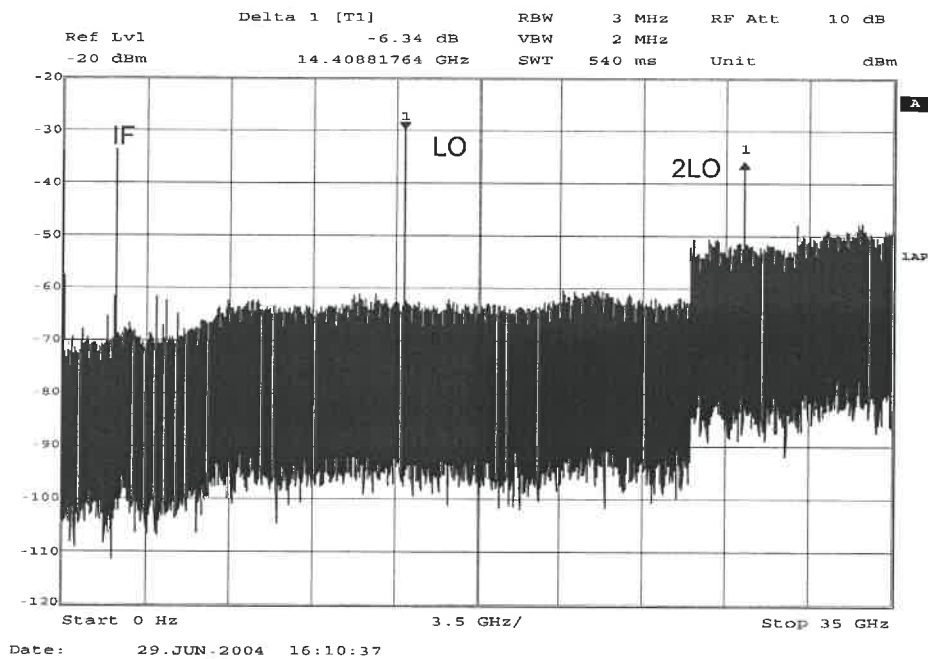


Fig.2.12 Oscillating and mixing spectrum of the conventional SOM

2.4 SIW Cavity Design

A rectangular waveguide cavity, shown in Fig.2.13, is constructed with width a , height b and length d , which means short-end waveguide at $z=d$. When d is the integral number times of the half waveguide length ($d=n\times\lambda_g/2$, $n=1,2,3\dots$), the electromagnetic wave will be reflected by the short-end to produce a standing wave and to make a null electric field at the other end ($z=0$) of the waveguide. It would not change the original field distribution when an electric wall is introduced at $z=0$, thus leading to a rectangular cavity. Electric and magnetic energy is stored within the cavity, and some power can be dissipated in the metallic walls of the cavity, as well as in the dielectric material that is filled in the cavity.

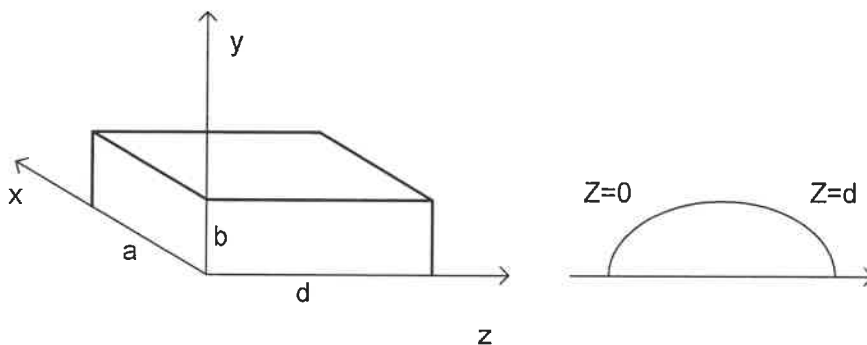


Fig.2.13 Rectangular waveguide cavity

The SIW cavity was first described by Cassivi in [13]. As shown in Fig.2.14, this kind of cavity is built in a substrate by using rows of via holes and the energy is coupled by coplanar waveguides. There are two predominant characteristics of SIW cavity as those of metal cavity: one is the resonant frequency, the other is the Q factor.

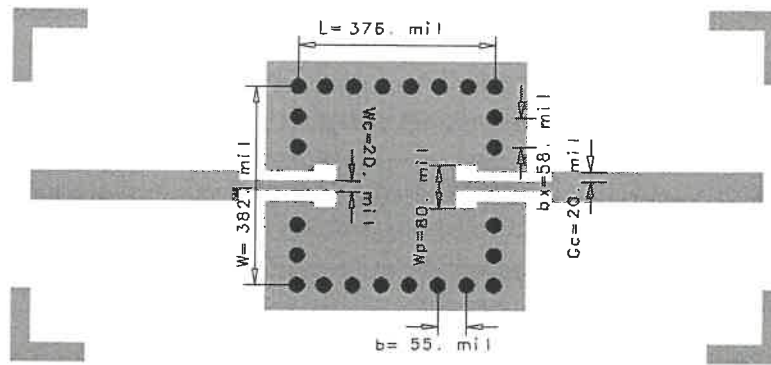


Fig.2.14 CPW coupling topology of an SIW cavity

The resonant frequency of SIW Cavity (TE_{m0l}) is determined by the formula in [13]:

$$f_{m0l} = \frac{c}{2\sqrt{\epsilon_r}} \sqrt{\left(\frac{m}{W_{eff}}\right)^2 + \left(\frac{l}{L_{eff}}\right)^2} \quad (2.2)$$

where

$$L_{eff} = L - \frac{D^2}{0.95b} \quad (2.3)$$

$$W_{eff} = W - \frac{D^2}{0.95b_x} \quad (2.4)$$

In this design, the cavity was constructed with Duroid 5870 substrate with dielectric constant as 2.33 and thickness at 20 mil. As sketched in Fig.2.14, the dimension of the cavity are $L=376$ mil, $W=382$ mil, $D=31$ mil, $b=55$ mil, $b_x=58$ mil. So the effective size of the cavity and its resonant frequency are $L_{eff}=358$ mil, $W_{eff}=365$ mil and $f_{101}=15.14$ GHz. The measured S-parameters of the SIW cavity are shown in Fig.2.15,

which demonstrates an insertion loss level of 0.757 dB at the resonant frequency of 14.46 GHz. There is 4.7% error between the calculated resonant frequency and the measured result. Compared with the results given in [13], the large error is caused by the coplanar waveguide design. The inset length of coplanar waveguide within SIW cavity greatly affected the resonator frequency. In this design, the outputs of the SIW cavity are connected with 50 Ω microstrip line with 60 mil width, but the CPW energy coupling circuit uses $W_c = 20$ mil microstrip lines. The discontinuity, caused by connecting lines of different width also has a slight effect on the response of the SIW cavity.

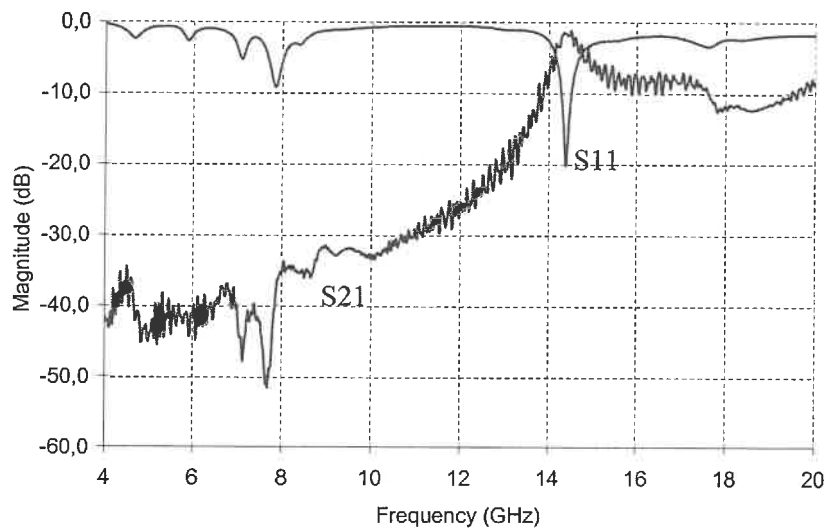


Fig.2.15 Insertion loss and return loss measurement of SIW cavity

The unloaded quality factor of the cavity is defined by the ratio between stored energy and lost power, and is approximated by the relation [14]:

$$\frac{1}{Q_u} = \frac{1}{Q_c} + \frac{1}{Q_d} \quad (2.5)$$

$$Q_c = \frac{(kad)^3 b \eta}{2\pi^2 R_s} \frac{1}{2a^3 b + 2bd^3 + a^3 d + ad^3} \quad (2.6)$$

$$Q_d = \frac{1}{\tan \delta} \quad (2.7)$$

where

$$a = W_{eff} = 365 \text{ mil} = 9.27 \text{ mm} ;$$

$$d = L_{eff} = 358 \text{ mil} = 9.09 \text{ mm} ;$$

$$b = H = 20 \text{ mil} = 0.51 \text{ mm} .$$

The conductivity of copper is $\sigma = 5.813 \times 10^7$ s/m, $\mu_0 = 4\pi \times 10^{-7}$ H/m. Then the surface resistivity is

$$R_s = \sqrt{\frac{\omega \mu_0}{2\sigma}} = 1.57 \times 10^{-2} \Omega .$$

The intrinsic impedance is

$$\eta = \frac{377}{\sqrt{\epsilon_r}} = 247.0 \Omega .$$

The wavenumber k is

$$k = \frac{2\pi f \sqrt{\epsilon_r}}{c} = 463.6 \text{ m}^{-1} .$$

So from formula (2.6) the Q due to conductor loss is:

$$Q_c = 1535 .$$

The Q due to dielectric loss, calculated from (2.7), is

$$Q_d = \frac{1}{\tan \delta} = \frac{1}{0.0012} = 833$$

Thus the total Q, can be found from (2.5) as

$$Q_u = \left(\frac{1}{1535} + \frac{1}{833} \right)^{-1} = 540$$

It is clear that the dielectric loss has the predominant effect on the Q factor of SIW cavity. The higher Q could be obtained using an air-filled cavity, but its three-dimension structure makes it quite difficult to integrate with printed circuits and active devices mounted on a substrate. Though the SIW cavity has a lower Q factor than an air-filled cavity, its easy integration with other printed circuits makes it as a low cost and high integration component in microwave and millimeter-wave applications.

The unloaded Q value of SIW cavity can also be obtained [15], by using its measured S-parameters. The loaded Q of cavity is defined as

$$Q_l = \frac{f_0}{\Delta f_{3-dB}} \quad (2.8)$$

where f_0 is the resonant frequency and Δf_{3-dB} is the 3-dB bandwidth. In this design,

$f_0 = 14.46$, $\Delta f_{3-dB} = 0.63$ GHz, Q_l is found equal to

$$Q_l = \frac{14.46}{0.63} = 22.95 \quad (2.9)$$

The external Q of the resonator Q_e , which includes the input-output loading effects, can be found from

$$S_{21} (dB) = 20 \log_{10} \left(\frac{Q_l}{Q_e} \right) \quad (2.10)$$

where S_{21} is equal to the measured insertion loss minus the loss of microstrip line that is connected between SIW cavity and the network analyzer. The loss of microstrip line is measured at 0.388dB. Then $S_{21} = 0.757 - 0.388 = 0.369$ dB.

Equation (2.10) gives

$$Q_e = Q_l \cdot 10^{S_{21}(dB)/20} = 23.946$$

After knowing Q_e and Q_l , we can find Q_u from

$$\frac{1}{Q_l} = \frac{1}{Q_u} + \frac{1}{Q_e} \quad (2.11)$$

And the Q_u of the SIW cavity is found to be equal to 552. The Q_u calculated by these two ways are close to the result given in [13]. An S-parameter model of the SIW cavity is built on the measured results, which is used as a component in the SIW SOM simulation.

2.5 Feedback SIW SOM Design

In the feedback SIW SOM design, the parallel CML is replaced by the SIW cavity. The schematic circuit of SIW SOM is quite similar to Fig.2.9, the only difference being to use the S-parameter model of SIW cavity to replace the parallel CML. The simulated open-loop gain and phase responses of the SIW SOM are shown in Fig.2.16. The simulation results indicate that the expected oscillating frequency is 14.4-GHz. After fine-tuning, the SIW SOM oscillated at a frequency of 14.2 GHz, which is a bit lower

than indicated by the measured open-loop responses shown in Fig.2.16. The layout of the SIW SOM, with size as 53 mm×34 mm , is shown in Fig.2.17.

As a 16 GHz RF signal is applied at the *RF Input* port, the mixing spectrum at *IF Out* is shown in Fig.2.18. There are many mixing signals and the wanted down-converted signal is

$$IF = RF - LO = 16GHz - 14.2GHz = 1.8GHz$$

The other mixing signals are

$$RF + LO = 16GHz + 14.2GHz = 30.2GHz$$

$$2LO - RF = 28.4GHz - 16GHz = 12.4GHz$$

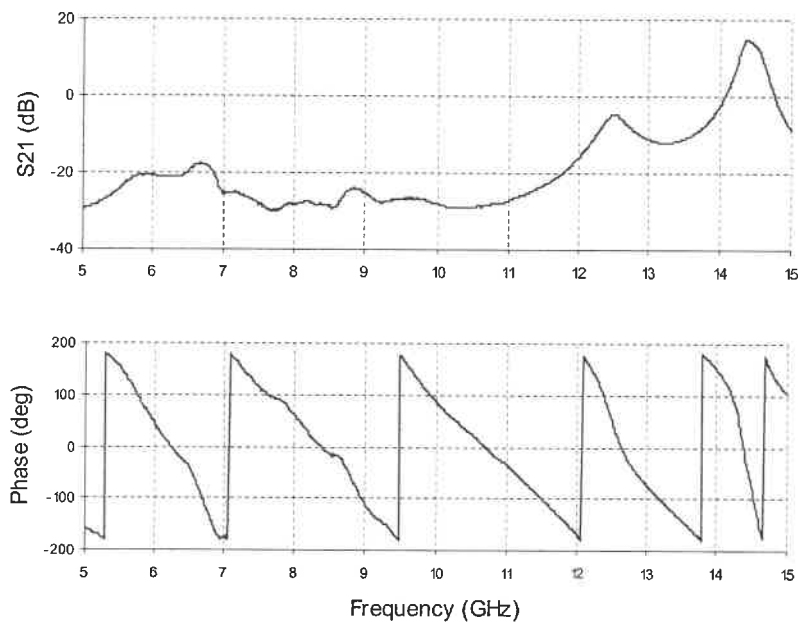


Fig.2.16 Open loop simulation of SIW SOM

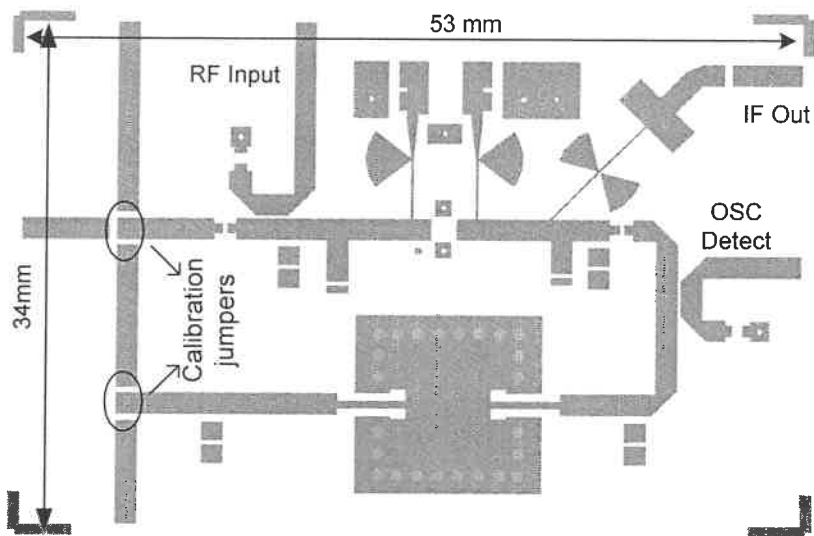


Fig.2.17 Layout of SIW SOM

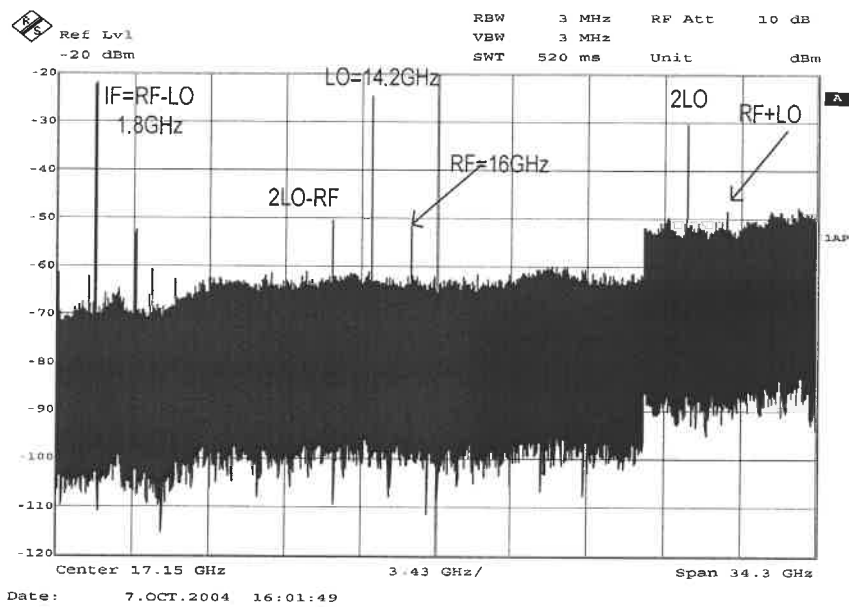


Fig.2.18 Spectrum of RF signal mixing with LO

When a 30 GHz RF signal is input from *RF Input* port, the circuit works as a sub-harmonic SOM, since in this case, the RF signal mixes with the second harmonic of the internal oscillation. Its mixing spectrum is shown in Fig.2.19 and the wanted down converted signal is

$$IF = RF - 2LO = 30GHz - 28.4GHz = 1.6GHz$$

The other mixing signal is

$$RF - LO = 30GHz - 14.2GHz = 15.8GHz$$

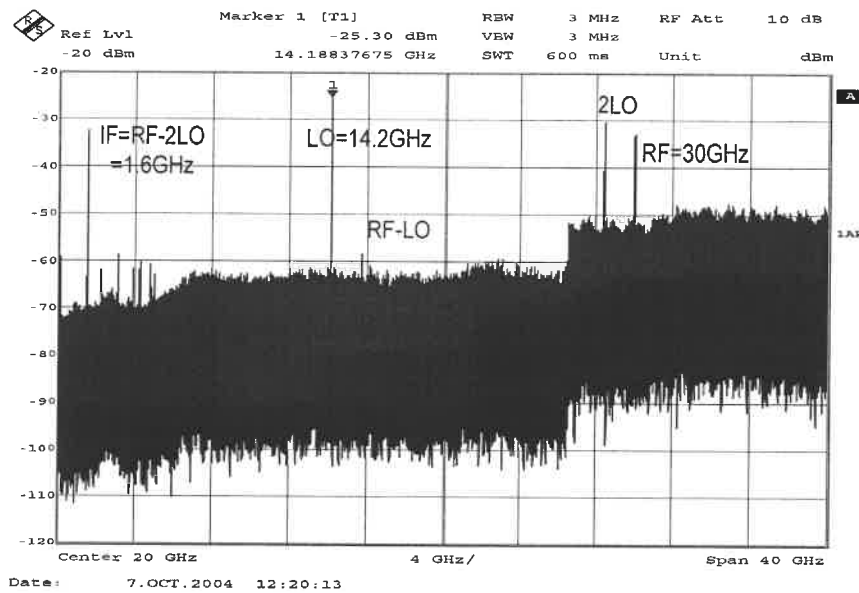


Fig.2.19 Spectrum of RF signal mixing with 2LO

2.6 Comparison of the IF Phase Noise

The design of SIW SOM is more complicated than the design of conventional SOM, because the SIW SOM needs additional simulation of the SIW cavity by three-dimensional HFSS electromagnetic simulator. But the SIW SOM provides advantage in phase noise because it uses the SIW cavity to stabilize the oscillating frequency.

Referring to [16], a standard noise figure computation of mixer is performed using the IEEE standard definition of single sideband noise figure:

$$NF_{ssb} = 10 \log \left(\frac{(v_n^2(f)/R) + kT_0(G_1 + G_2 + \dots + G_n)}{kT_0G_1} \right) \quad (2.12)$$

where

k is Boltzmann's constant (1.389658×10^{-23}),

T_0 is the IEEE standard temperature for noise figure (290 K),

G_1 is the conversion gain of the mixer,

G_2 is the image conversion gain of the mixer,

G_3, \dots, G_n are conversion gains of higher order mixing products,

R is the resistance of the output termination,

v_n is the noise voltage at the output port at the output frequency where the input and output terminations do not contribute any noise.

When the effects of LO phase noise is included, the $v_n^2(f)/R$ term is replaced with total noise power at the output integrated over a bandwidth B centered at the output IF frequency f_{IF} :

$$NF_{ssb} = 10 \log \left(\frac{\left(\int_{f_{IF}-B/2}^{f_{IF}+B/2} v_n^2(f) df / R \right) + kT_0(G_1 + G_2 + \dots + G_n)}{kT_0 G_1} \right) \quad (2.13)$$

Comparing (2.12) and (2.13), it is known that the LO will generate noise over a range of frequencies from $f_{LO} - B/2$ to $f_{LO} + B/2$. These will mix with the RF tone at f_{RF} to produce noise from $f_{IF} - B/2$ to $f_{IF} + B/2$, where $f_{IF} = |f_{RF} - f_{LO}|$. As a result, LO phase noise definitely affects the noise figure of mixer performance. Improving LO phase noise can result in a better noise figure for the mixing signal.

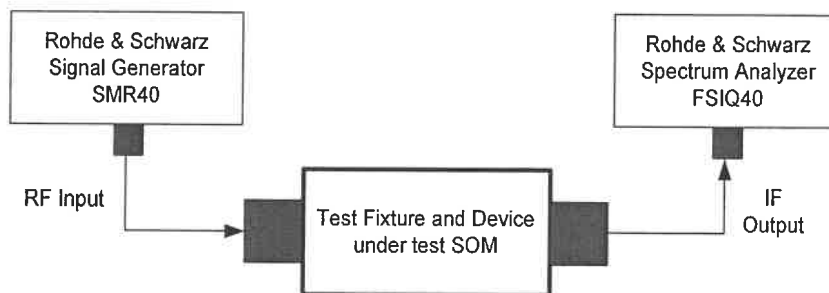


Fig.2.20 Experimental setup for measuring the IF phase noise of SOMs

Normally in a SOM design, the phase noise of the IF signal is measured instead of testing the phase noise of the oscillator. The measurement setup of the IF phase noise is

shown in Fig.2.20. The circuits under test are in a test fixture, the RF signal is input by a signal generator and at the output of the circuit, the IF signal is connected to a spectrum analyzer.

The IF phase noise of both conventional SOM and SIW SOM are measured and the saved in Fig.2.21 to Fig.2.24. The offset frequency is from 100 kHz to 100 MHz. Fig.2.21 is the IF ($IF = RF - LO$) phase noise of the conventional SOM with a 16 GHz RF input and Fig.2.22 is the phase noise of $IF = RF - 2LO$ in the conventional SOM with a 30 GHz RF input. Fig.2.23 shows the IF ($IF = RF - LO$) phase noise of the SIW SOM with a 16 GHz RF input and Fig.2.24 is the phase noise of $IF = RF - 2LO$ of the SIW SOM with a 30GHz RF input. The measured IF phase noise is listed in table 2.1.

Table 2.1 Comparison of IF phase noise for SOM and SIW SOM

offset frequency	Phase noise (dBc/Hz)			
	100 KHz	1 MHz	10 MHz	100 MHz
measurement 1 for SOM	-60	-100	-115	-115
measurement 2 for SOM	-60	-90	-115	-115
measurement 1 for SIW SOM	-80	-105	-130	-130
measurement 1 for SIW SOM	-70	-100	-120	-120

By comparing the phase noise pictures of the conventional SOM and the SIW SOM, it is very clear that SIW SOM provides a phase noise 10dB to 20dB less than the conventional SOM because SIW SOM applied a SIW cavity in the feedback loop to stabilize the oscillator frequency.

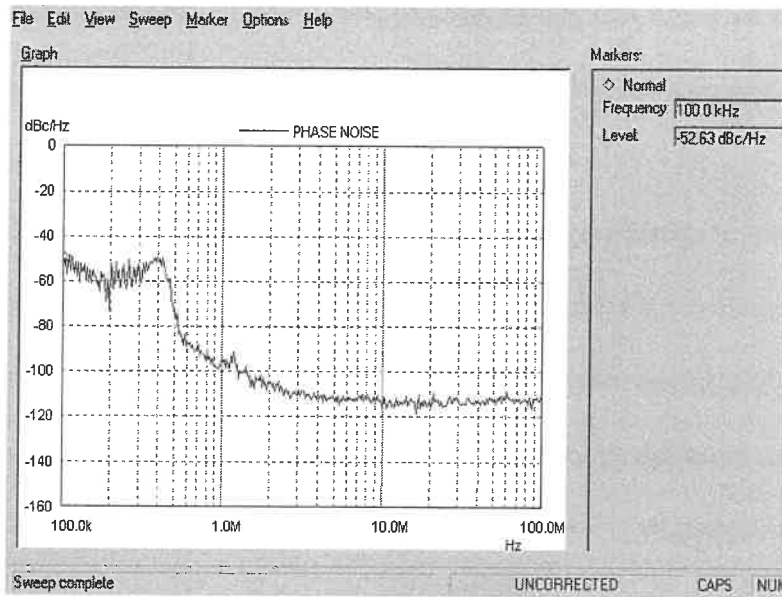


Fig.2.21 IF Phase Noise measurement 1 of the conventional SOM
(RF=16 GHz, IF=RF-LO)

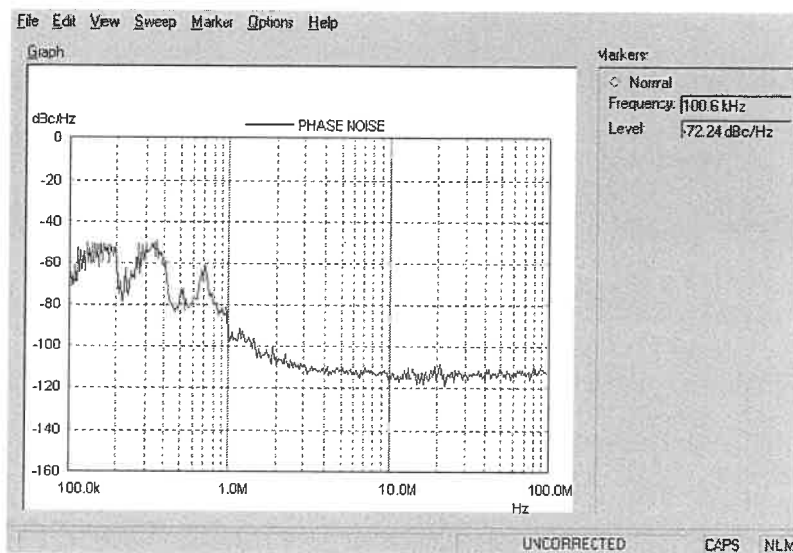


Fig.2.22 IF phase noise measurement 2 of the conventional SOM
(RF=30 GHz, IF=RF-2LO)

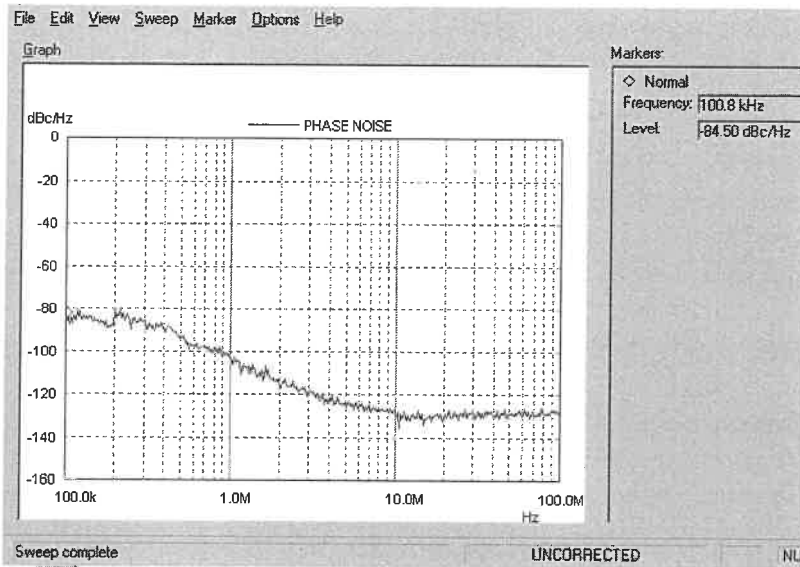


Fig.2.23 IF phase noise measurement 1 of the SIW SOM
(RF=16 GHz, IF=RF-LO)

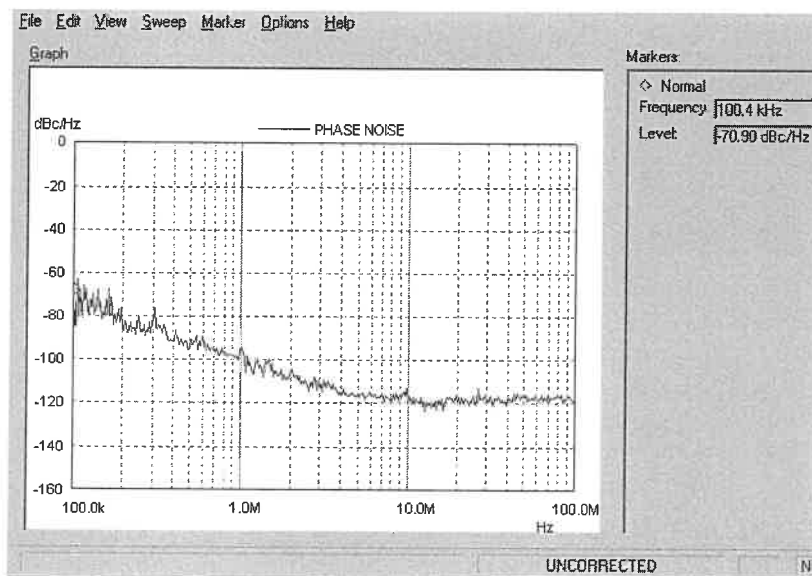


Fig.2.24 IF phase noise measurement 2 of the SIW SOM
(RF=30 GHz, IF=RF-2LO)

2.7 Summary

In this chapter we mainly design two kinds of SOM and compare their phase noise performance. One is the conventional design with the parallel CML as feedback loop, and the other is the SIW SOM using SIW cavity as the resonator.

The working concept of the feedback SOM is simulated by ADS at the beginning of this chapter, and the simulated results indicate that the strong feedback would drive active device into saturation, which makes the mixing and oscillating functions occur simultaneously.

Then, a linear model of the ATF36077 is built, using TRL calibration technique and small signal S-parameter measurement. A 14 GHz linear amplifier is designed on that model. The good match between the measured and simulated results proves that the built model of the ATF36077 is accurate in a linear DC bias condition.

A conventional feedback SOM with the paralleled CML cascaded with the amplifier was designed. A new SOM structure was proposed by replacing paralleled CML with an SIW cavity. The mixing spectrums of the SIW SOM demonstrated.

At the end of this chapter, the IF phase noise of these two SOM circuits are measured and compared. The results indicate that SIW SOM provides a phase noise with 10dB to 20 dB less than that of the conventional SOM.

Though SIW SOM has a good phase noise performance, its design needs a lot of fine tuning to make it work well. The picture of SIW SOM is shown in Fig.2.25, four tuning stubs were added to the circuit.

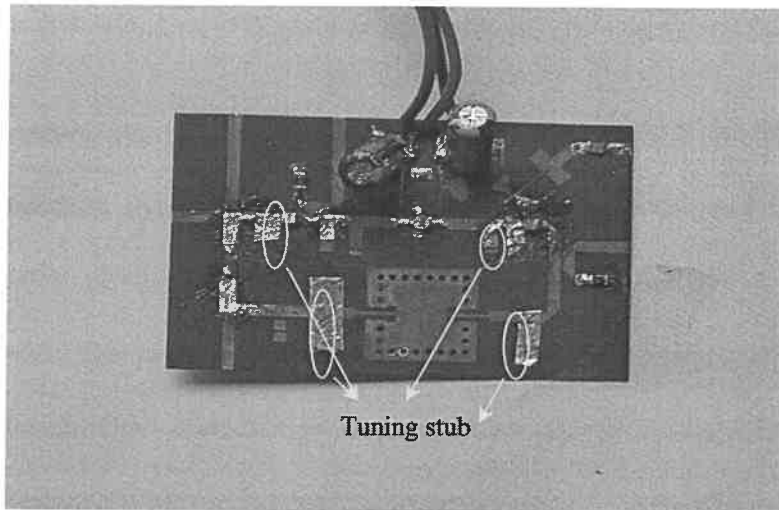


Fig.2.25 SIW SOM circuit

CHAPTER 3

SUBHARMONIC SIW SOM DESIGN WITH INTEGRATED PATCH ANTENNA

3.1. Introduction

The first subharmonic SOM [20] was operated at 34 GHz with 5% conversion efficiency and -121.6dBm/Hz detection sensitivity at Doppler frequency of 4 kHz. A 77-GHz MMIC subharmonic SOM using pHEMT with 12dB conversion loss was proposed in [5]. And a balanced integrated-antenna subharmonic SOM at 60GHz, with 15dB conversion loss was presented in [3].

In this chapter, a subharmonic SIW SOM integrated with a patch antenna is presented. The whole design combines the SIW SOM circuit shown in chapter 2 and a patch antenna into one planar circuit, which functions as an antenna-integrated receiver. A 30 GHz patch antenna is placed at the gate of the AFT36077. As a result, a 30 GHz signal received by the patch antenna can mix with the second harmonic internally oscillation, to produce a 2 GHz IF frequency at the IF port. The subharmonic SIW SOM integrated with antenna is a simple receiving circuit, which can be applied for millimetre-wave communication systems, such as imaging radars, Doppler radar sensors, transponders, and so on.

Subharmonic SOMs using second harmonic LO to mix with RF signal, which have some advantages as follow:

1. Subharmonic SOM can use FETs with f_{\max} less than RF frequency, which reduces the choice limitation of FETs.
2. Injection locking can be avoided in subharmonic SOM, because the antenna network acts as a total reflection at the LO frequency and has less effect on the oscillation.
3. The design of subharmonic SOM is low in cost, easy in fabrication.

3.2. Patch Antenna Design

3.2.1 Simulation of Patch Antenna

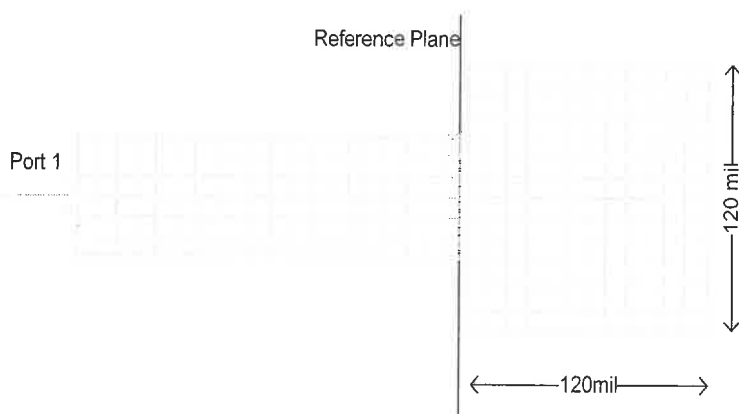
Antenna is an essential component in wireless communication systems and microwave antennas are widely used in radars, satellite communications, LMDS (Local Multipoint Distribution Service) and so on. According to IEEE standard 145-1973, an antenna is “a means for radiation or receiving radio waves [17]”. Microstrip antennas are widely used to microwave and millimeter-wave frequency, because they are low-cost, light-weight, compact and easy to manufacture. They can be easily integrated with feed networks, matching networks, phasing networks, switch networks, and filters, all of which are realized by solid-state devices [18]. Their directivity, however, is in low efficiency and narrow bandwidth.

As a planar three-dimension structure, often labeled 2.5D, the patch antenna can be simulated by using ADS-MoM. The substrate used to make the patch antenna is RT5870 with dielectric constant $\epsilon_r = 2.33$, thickness $t = 20\text{mil}$, which is the same as the SIW

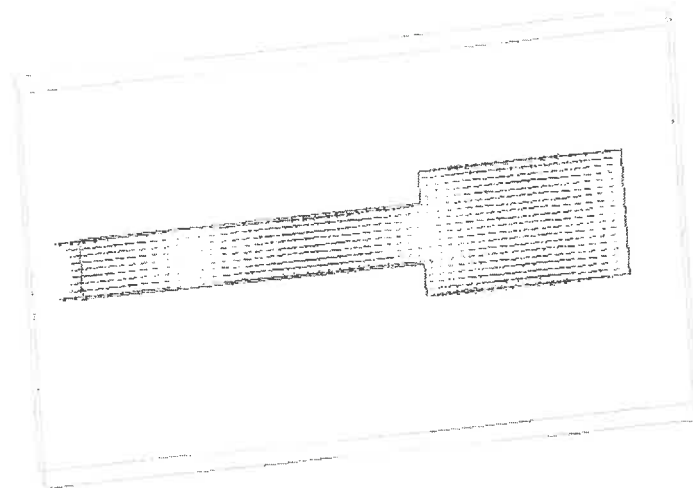
SOM circuit used. The first step is to determine the dimension of a 30 GHz patch antenna from the equation (3.1), as:

$$L = W = 0.49 \frac{\lambda}{\sqrt{\epsilon_r}} = 126\text{mil} \quad (3.1)$$

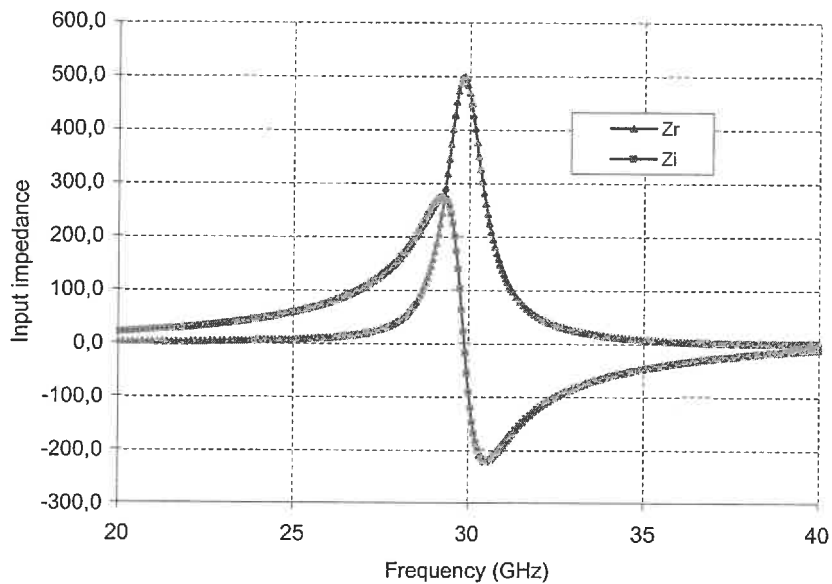
The structure of the patch antenna was drawn and simulation was done, as shown in Fig.3.1 (a). In order to test the input impedance of the patch antenna, the reference plane of port1 should be offset close to the edge of patch. By adjusting the calculated value of L and W from 126mil to 120mil, the zero reactance of input impedance shifts to 30-GHz, which demonstrates that the patch antenna with 120mil×120mil is resonant at 30-GHz. The simulated input impedance $Z_r + jZ_i$ is drawn in Fig.3.1 (c), which clearly demonstrates that at about 30 GHz, the imaginary part of input impedance is zero and the real part as high as 500 Ω . Fig.3.1 (b) shows the current distribution as a standing wave for the patch antenna at its resonant frequency.



(a) Mesh of simulated patch Antenna with offset reference plane



(b) Stand wave distribution of patch antenna



4.1(c) Simulation of Input Impedance

Fig.3.1 Simulated results of patch antenna without the affection of feed

There are many ways to feed the patch antenna such as probe feed, quarter-wave transformer edge feed, inset microstrip feed, microstrip edge gap feed, two-layer feed

and aperture coupled feed. In this design, the inset microstrip feed is chosen because of its planar structure as shown in Fig.3.2. A matching network is necessary to match the 500Ω input impedance of the antenna to a 50Ω feed line. In fact, the inset part can work as a voltage transformer to match the two different resistances. The size of patch needs to be adjusted after adding the inset microstrip feed line, and the final dimensions of the patch is changed to $L = 123\text{mil}$, $W = 156\text{mil}$.

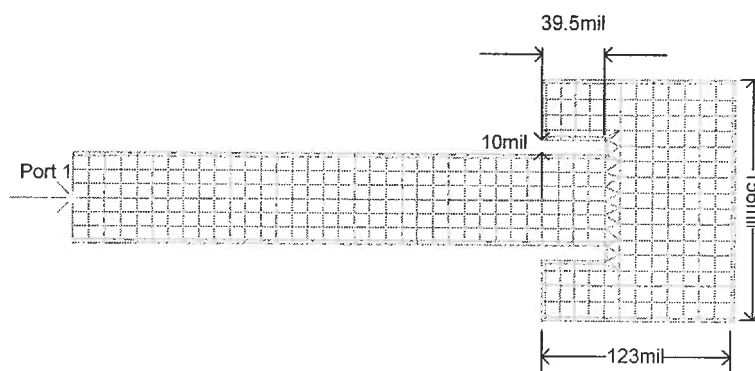


Fig.3.2 Patch antenna with inset microstrip feed

3.2.2 Measurement of Patch Antenna

It was indicated in [19] that antenna measurement techniques are separated in two sides: the parameters that characterize an antenna on the circuit side are its input impedance (match, SWR, reflection coefficient); and on the radiation side, the relevant parameters are the gain, the efficiency, the radiation pattern and the polarization.

Network Analyzer is the instrument most frequently used to measure microwave circuits and devices. It is also used, on an antenna circuit side, to measure the S-parameter of the patch antenna. Fig.3.3 is the test setup for measuring input impedance,

with one port connected with vector network analyzer through a test fixture, and the other port of antenna points toward the open space. Fig.3.4 shows the measured return loss of the patch antenna at the frequency range from 20 GHz to 40 GHz. As shown the resonant frequency is slightly lower than 30 GHz, at which -30 dB return loss achieved. The bandwidth of the patch antenna is about 5%. The measured result is saved as S-parameter model would be used in system simulation at the next design step– integrated SIW SOM with patch antenna.

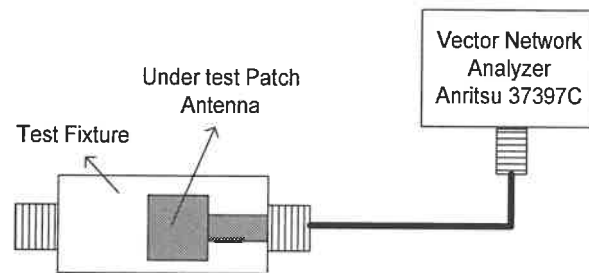


Fig.3.3 Experimental setup for measuring input impedance

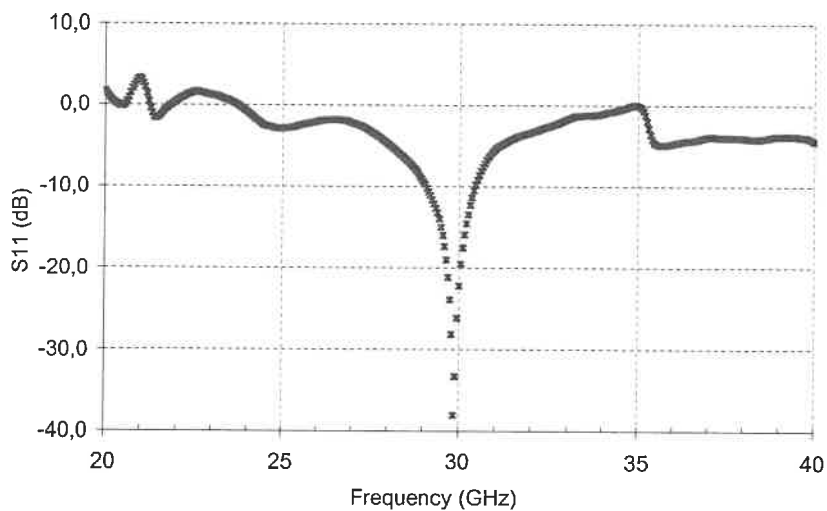


Fig.3.4 S-parameter measurement of patch antenna

On the radiated wave side, the main parameters to be measured are radiation pattern, antenna gain and antenna polarization. An antenna chamber is usually used to test these characteristics of antennas. The test setup for antenna radiation parameters measurement is shown in Fig.3.5. The whole setup, except for the computer and analyzer, are settled in antenna chamber. Two antennas are needed to determine the pattern: one is the antenna under test (AUT), the other is the known gain antenna. The AUT is mounted on an electromechanical system with one or more degrees of freedom. The known gain antenna transmits signal to a target, and the AUT receives the signal reflected from the target. The AUT rotates to test different patterns.

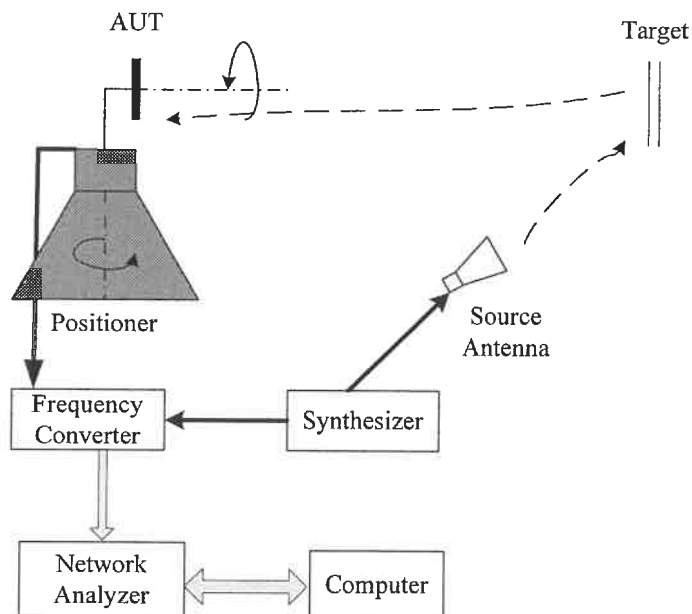


Fig.3.5 Test setup for antenna parameters measurement

When the patch antenna lies in xy -plane and the feed along the x -axis, the E-plane is in xz -plane :

$E_{\theta}(\theta, \phi = 0^{\circ})$ = pattern of θ component as a function of θ in the $x-z$ plane ($\phi = 0^{\circ}$).

The H-plane is in yz -plane :

$E_{\theta}(\theta, \phi = 90^{\circ})$ = pattern of θ component as a function of θ in the $y-z$ plane ($\phi = 90^{\circ}$).

In each plane, the co-polarization and cross-polarization are measured respectively. In antenna measurement, co-polarization means the transmission antenna transmits the wave in parallel polarization with the antenna under test; and cross-polarization means the transmission antenna transmits the wave in orthogonal polarization with the AUT polarization. In practice, cross-polarization should be 15 dB to 20 dB less than co-polarization. The measured radiation patterns are shown in Fig.3.6, which are close to the simulated results. The gain of the patch antenna is around 5 dB. The ripple in E-plane pattern is partly caused by asymmetric structure along x axis and partly caused by the radiation from the feed line. The substrate with 20mil thickness used to design 30 GHz antenna may be too thick for the 50Ω microstrip feed line, and produces uncontrolled radiation at the feed line. However, the 20mil thick RT5870 is chosen, because it is hard enough without being metal based, which allows for quick circuit manufacturing. The frequency responses of E-plane and H-plane patterns are shown in Fig.3.7 and Fig.3.8 respectively.

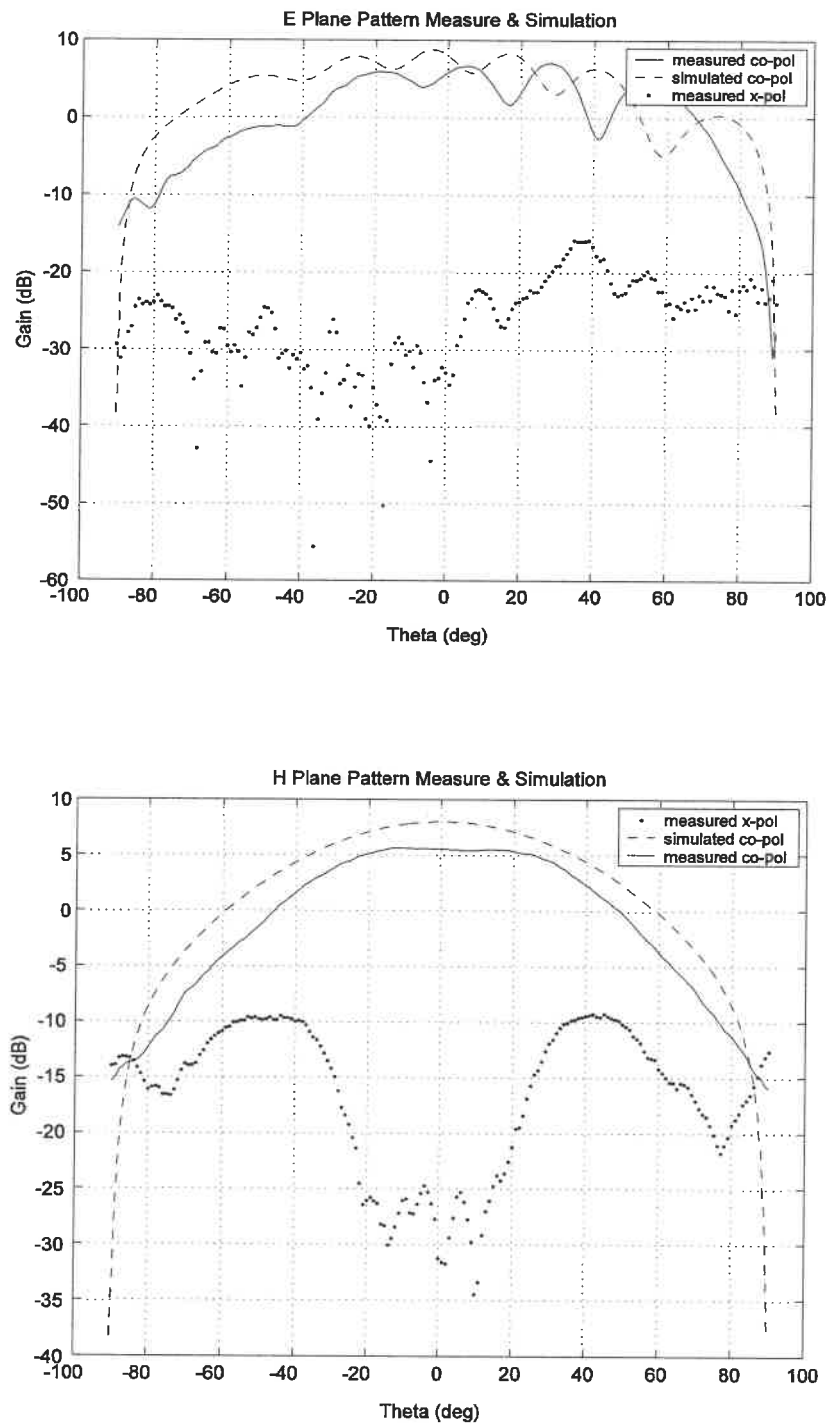


Fig.3.6 Simulated and measured pattern of principle planes

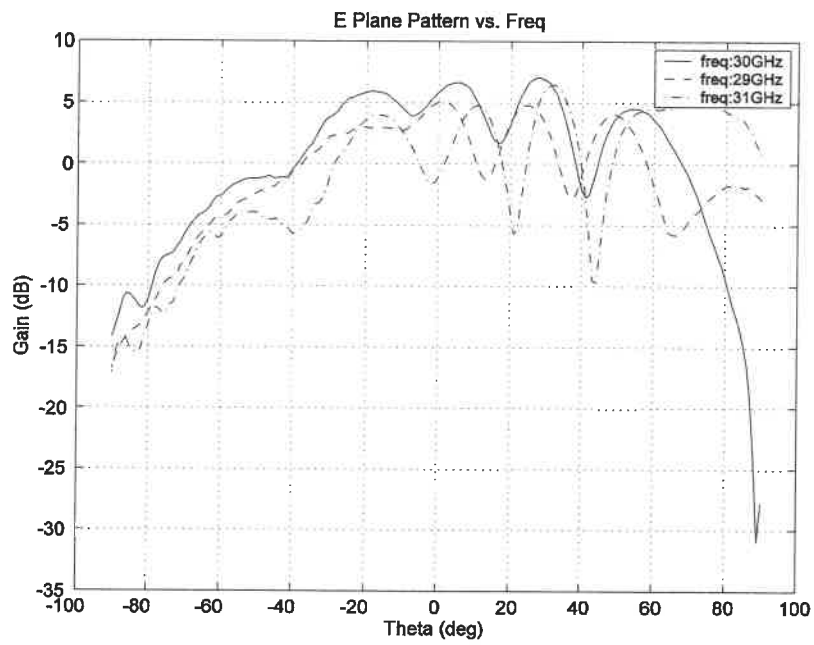


Fig.3.7 Measured frequency response of the E plane pattern

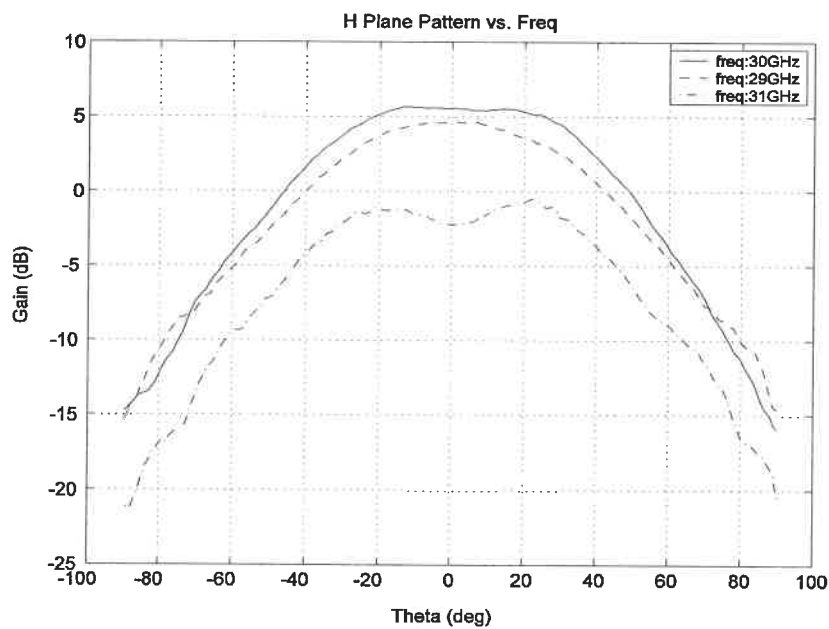


Fig.3.8 Measured frequency response of the H plane pattern

3.3. Improved Design of SIW SOM

As discussed in Chapter 2, a feedback SIW SOM circuit includes an amplifier and a feedback resonant-SIW cavity. Lots of tuning are needed in that SIW SOM circuit, because both the amplifier and the SIW cavity have a sharp frequency response. Fig.3.9 demonstrates the measured S_{21} of the amplifier and the SIW cavity designed in Chapter 2. The amplifier is designed as conjugate match of the transistor by using ADS, and the SIW cavity is simulated by HFSS. It is very difficult to tune these two components at the same frequency. Therefore, when the amplifier is cascaded with the SIW cavity, lots of efforts are required to tune the circuit and make it works at the design frequency. So we wonder if the amplifier is necessary for the SIW SOM design.

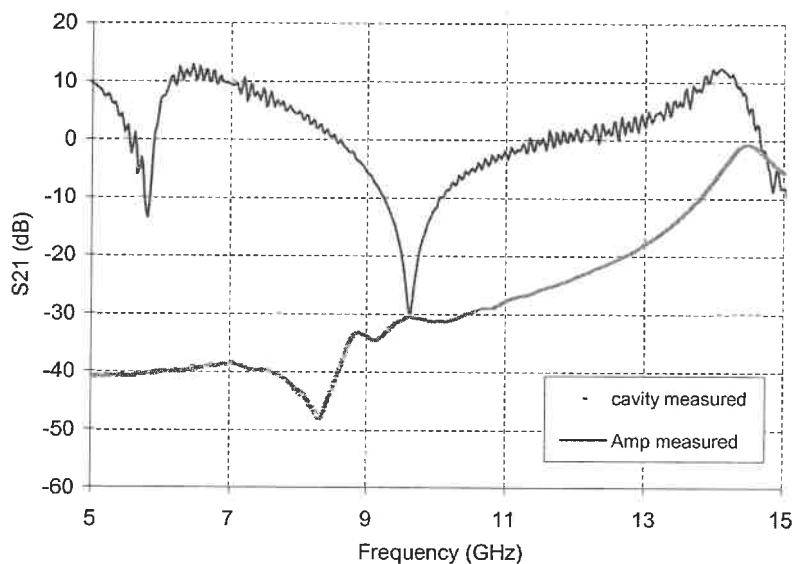


Fig.3.9 Measured S_{21} of the amplifier and the SIW cavity

In fact, since the SIW cavity itself has a very good frequency response, there is no need to design FET as an amplifier in an SIW SOM design. A typical frequency response of a SIW cavity is shown in Fig.2.17, which exhibits that the SIW cavity presented as 50Ω loads solely at the resonator frequency, while at other frequency, it acts as a total reflector. Therefore, as a transistor connected with the cavity, the FET is terminated with 50Ω loads only at the resonant frequency, while at other frequencies, the FET is terminated with the reflective loads. In other words, it appears that the SIW cavity works as a filter in the design. Within the passband of the cavity, the S_{21} of the cascade has a gain, while beyond the passband the S_{21} exhibits a loss. It can be presumed that the loop gain of ATF36077 connected with SIW cavity directly would show a good response required in the feedback SOM design and Fig.3.10 demonstrates its simulated open loop responses. The loop gain higher than 0dB only happens around 14 GHz, and it is easy to realize the oscillation frequency by controlling the phase shift of the open loop response.

The layout of the subharmonic SIW SOM integrated with the patch antenna is shown in Fig.3.11. The 30 GHz patch antenna is connected to the gate of the ATF36077. The measured open loop gain and phase response are shown in Fig.3.10. There is a good agreement between the simulated and measured responses throughout the band. The picture of the constructed circuit is shown in Fig.3.12. No tuning stubs to adjust responses of the circuit were needed. The good agreement between simulated and measured responses with no additive tuning stubs verifies that the improved design

technique (connecting FET with SIW cavity directly) is better than the technique (connecting SIW cavity with a FET designed as an amplifier) used in Chapter 2.

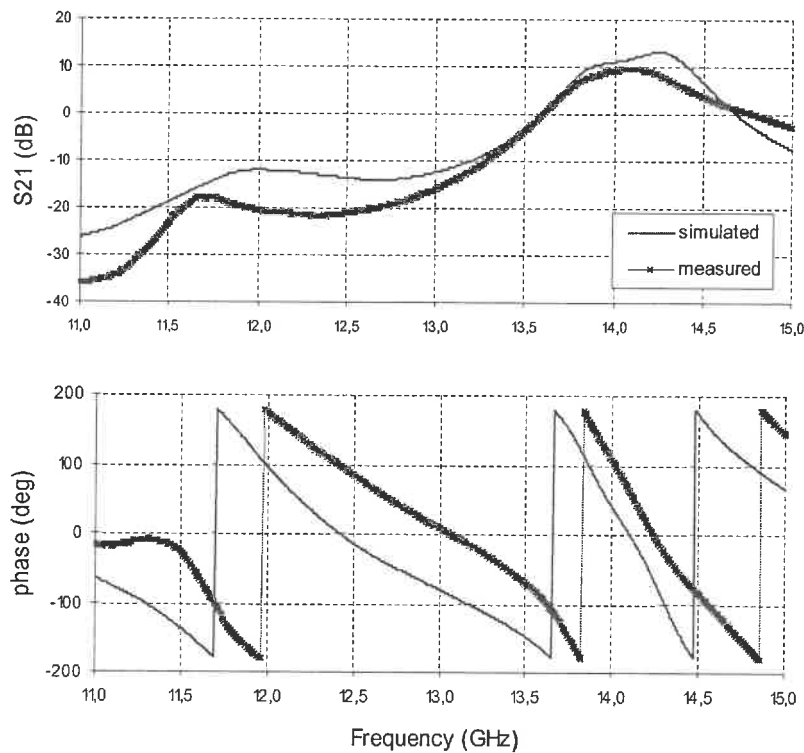


Fig.3.10 Simulated and measured open loop response of ATF36077 cascaded with SIW Cavity

Once the loop is closed, an oscillator happens at 14.347 GHz with the second harmonic is 28.684 GHz. A 30.4 GHz signal is transmitted by a horn antenna to the patch antenna, and the received signal mixes with the second harmonic oscillation. The mixing spectrum of the whole circuit is shown in Fig.3.13. The fundamental oscillating frequency is a little bit higher than the indication of the measured open-loop results. The mixing signals include second order (RF-LO), third order (RF-2LO), fourth order (3LO-RF) and sixth order (2IF) mixing frequency.

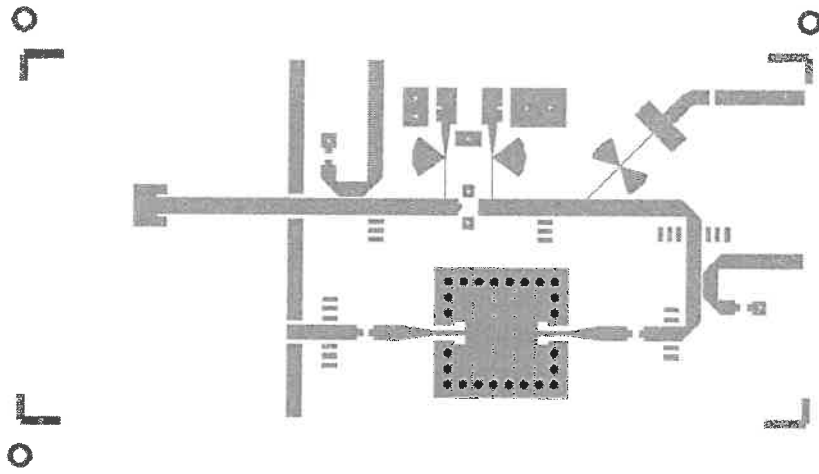


Fig.3.11 Layout of SH SIW SOM integrated with patch antenna

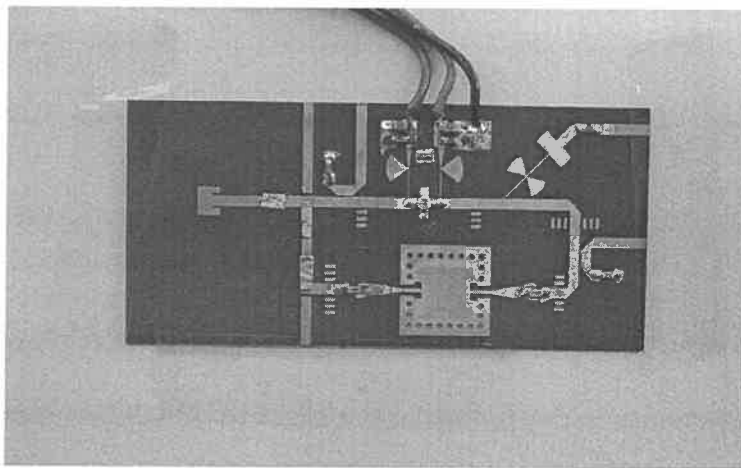


Fig.3.12 SH SIW SOM integrated with patch antenna circuit

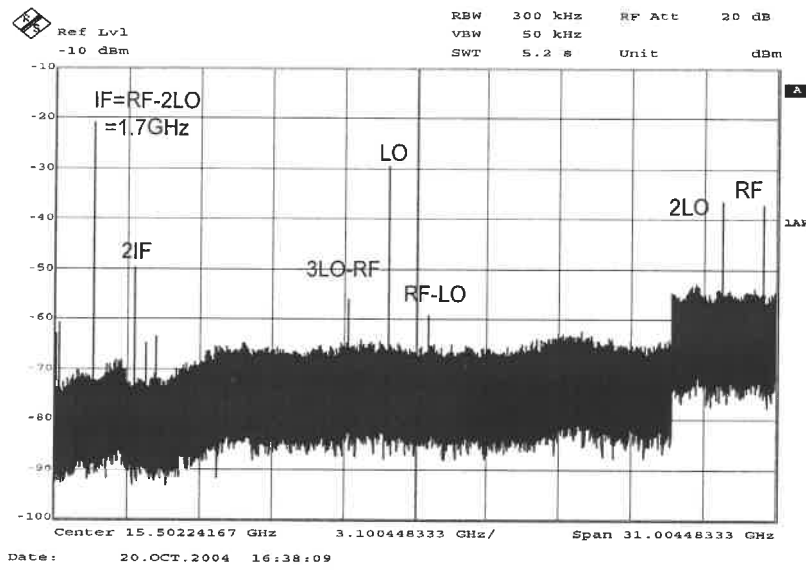


Fig.3.13 Mixing spectrum of SH SIW SOM

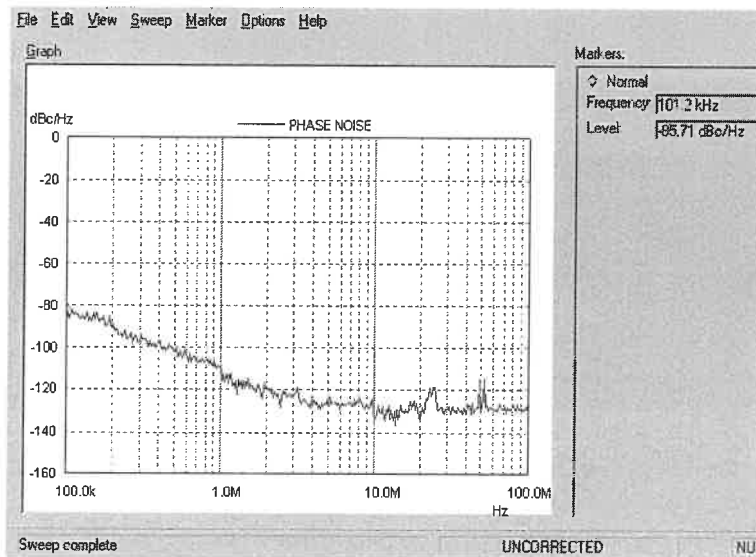


Fig.3.14 Measured IF phase noise of SH SIW SOM

Using the same way as described in Chapter 2, the IF phase noise of the subharmonic SIW SOM is measured by using spectrum analyzer (FSIQ40). The measured result is shown in Fig.3.14: as $-85\text{dBc/Hz @ } 100 \text{ kHz}$; $-115\text{dBc/Hz @ } 1 \text{ MHz}$; $-130\text{dBc/Hz @ } 10\text{MHz}$. This phase noise is better than both measured results for the SIW SOM designed in Chapter 2 (as shown in Fig.2.24 and Fig.2.25). The SIW SOM described in Chapter 2 has designed the ATF36077 as a conjugate match amplifier with a narrow band gain response. In fact, the amplifier itself can oscillate by connecting its input and output. The loop phase response is too sensitive to determine whether the oscillation comes from the amplifier plus delay line or from the SIW cavity plus delay line. What we wanted in the SIW SOM design is the zero phase shift to occur at the resonant frequency of the SIW cavity. The design in Chapter 2 cannot guarantee this key point, and in fact the oscillating affects by the amplifier and the SIW cavity simultaneously. Therefore, the IF phase noise is not only determined by the cavity, but also affects by the amplifier. The new design technique can guarantee the oscillating frequency is determined only by the resonant frequency of the SIW cavity. That is why the new circuit designed in this chapter can obtain better phase noise performance than the design in Chapter 2.

3.4. Mismatch Analysis

As the FET is connected with SIW cavity directly, the mismatching of the cascaded circuit is unavoidable, so this section discusses the port mismatching in the design. The input and output scattering parameters of the cascade are measured and plotted on a

Smith chart, as shown in Fig.3.15. Marker 1 and marker 2 are the input and output reflection coefficients at phase zero crossing frequency of 14.3 GHz respectively. $S_{11} = 0.102\angle 79.46$, $S_{22} = 0.54\angle 138.6$. Since the input and output impedance of the cascade are not exactly equal to Z_0 , the reflection between each other, when they are connected, would reduce the loop gain below the maximum available value. The real loop gain can be calculated by formula:

$$G = \frac{1 - |\Gamma_s|^2}{|1 - \Gamma_{in}\Gamma_s|^2} |S_{21}|^2 \frac{1 - |\Gamma_L|^2}{|1 - S_{22}\Gamma_L|^2} \quad (3.2)$$

where,

$$\Gamma_{in} = S_{11} + \frac{S_{12}S_{21}\Gamma_L}{1 - S_{22}\Gamma_L} \quad (3.3)$$

Assuming the reverse isolation of the ATF36077 is adequate, which means S_{12} can be ignored, then $\Gamma_{in} = S_{11}$, $\Gamma_{out} = S_{22}$; the loop gain takes the mismatch into account is simplified as:

$$G = \frac{1 - |S_{22}|^2}{|1 - S_{11}S_{22}|^2} |S_{21}|^2 \frac{1 - |S_{11}|^2}{|1 - S_{11}S_{22}|^2} \quad (3.4)$$

In our design, the measured open loop gain shown in Fig.3.10 is 7.5dB, the open loop gain includes the mismatching, by using formula (3.4), is:

$$G = 0.65 \times 5.62 \times 0.91 = 3.32 = 5.2dB \quad (3.5)$$

In this case the mismatching reduces the open loop gain by 2.3 to 5.2dB.

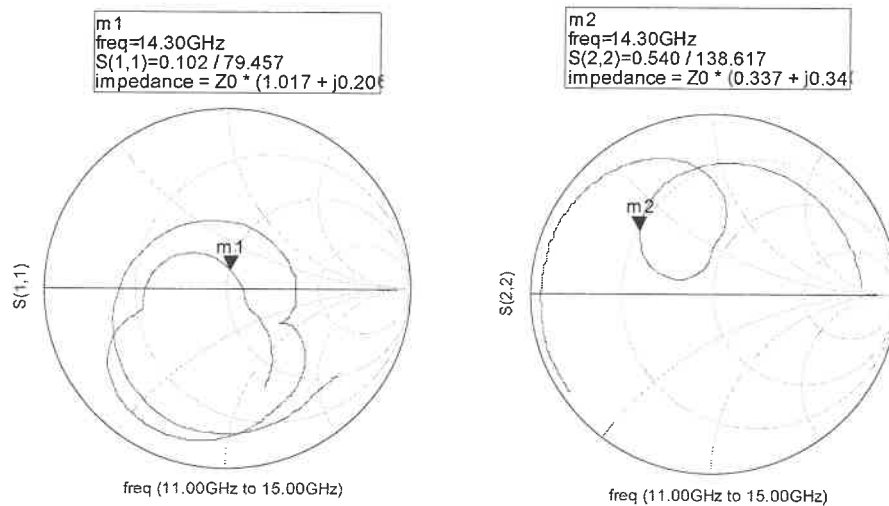


Fig.3.15 Input and output reflection of SH SIW SOM

3.5. Phase Noise Performance of SIW SOM

Phase perturbations, due to noise or parameters variations, results in a frequency shift at the output of the oscillators. Even a small noise into an oscillator leads to dramatic change in its frequency spectrum and timing properties. The asymptotic phase noise versus offset frequency is shown in Fig.3.16. The single side band (SSB) phase noise of an oscillator has -30dB/decade slope at offset frequencies below the flicker corner, and a slope of -20dB/decade at offset between the flicker corner and the resonator half-bandwidth, $f_o/2Q_l$. Above the resonator half-bandwidth, the SSB phase noise is flat.

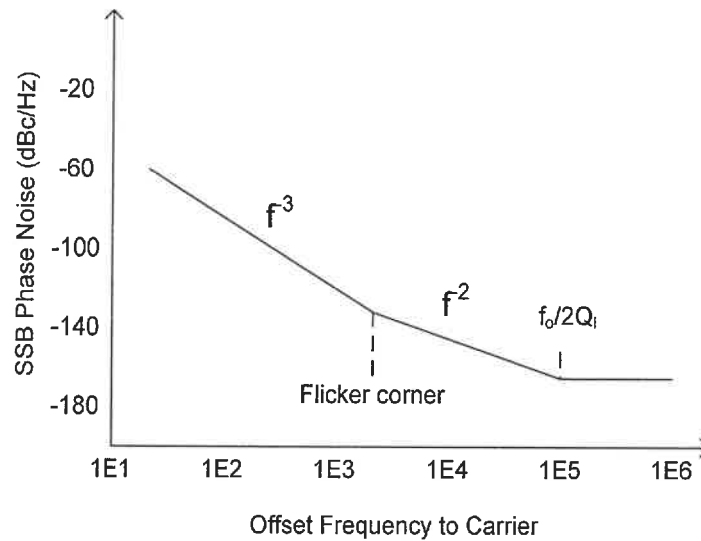


Fig.3.16 Oscillator SSB phase noise as a function of offset frequency to carrier

D. B. Leeson first summarized the phase noise characteristics of an oscillator constructed by cascading the amplifier with a resonator in [21]. The expression for oscillator SSB phase noise from Leeson is

$$L(f_m)(dBc/Hz) = 10 \log \left[\frac{1}{2} \left(\left(\frac{f_o}{2Q_l f_m} \right)^2 + 1 \right) \left(\frac{f_c}{f_m} + 1 \right) \left(\frac{FkT}{P_{osc}} \right) \right] \quad (3.6)$$

where,

$k = 1.38 \times 10^{-23}$ Joule/Kelvin — the Boltzmann constant,

$T = 293$ K (at room) — absolute temperature,

f_o = operation frequency (carrier frequency),

Q_l = loaded Q factor of the resonator,

f_m =offset frequency under test,

f_c =corner frequency of flicker noise,

P_{osc} =average power at oscillator output.

Formula (3.6) indicates the phase noise of feedback oscillator is inversely proportional to the square of the loaded Q factor. In fact, the loaded Q is a direct indication of many oscillator performance parameters. A high loaded Q can reduce phase noise, reduce frequency drift and isolate performance from active-device variation. Drift is reduced because the resonator solely determines the oscillation frequency in high-Q designs. Isolating the resonator from active device reactance reduces the effect of the temperature. A 34 GHz SOM using a distributed LC as a resonator was presented in [20] and its second LO had a phase noise of -70 dBc/Hz@100 kHz. A 60 GHz harmonic balanced SOM with DR as resonator was designed in [3], and had IF phase noise of -95 dBc/Hz@100 kHz. The IF phase noise of the 30 GHz subharmonic SIW SOM stabilized by the SIW cavity is -85.7 dBc/Hz@100kHz. In all these design, the phase noise is determined by the loaded Q of the resonators used in the circuits. As the phase noise performance of the SIW SOM is better than that of the SOM presented in [20], it can be said that the SIW cavity resonator has a higher Q factor than that of the distributed LC resonator. Since DR has the highest Q factor, the best phase noise result is achieved in [3].

The phase noise of SIW SOM working at a higher frequency can be predicted by using formula (4.5). A 28 GHz SIW cavity, designed in same substrate

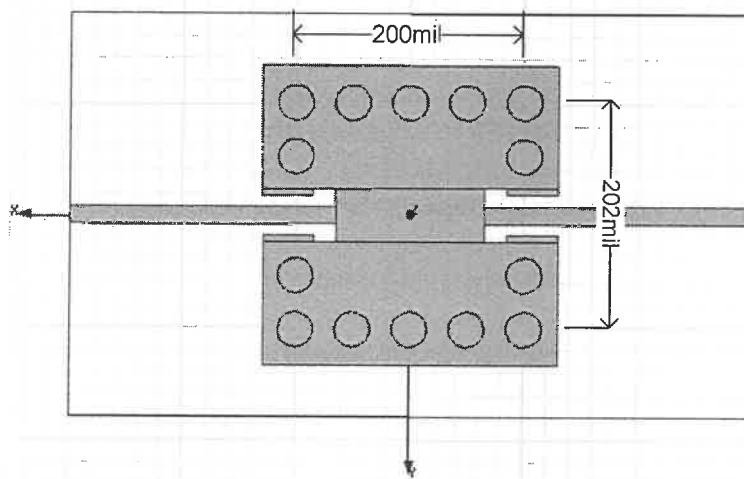
(RT5870, $\epsilon_r = 2.33$, $H=20\text{mil}$), was simulated by Ansoft. The layout and the simulated S-parameters are shown in Fig.3.17. The figure demonstrates that the resonant frequency is 28.7 GHz with 0.37dB insertion loss; the 3dB bandwidth range from 29.7 GHz to 27.9 GHz. The loaded Q of the SIW cavity is calculated by formula (2.8) as:

$$Q_l = \frac{f_0}{\Delta f_{3-dB}} = \frac{28.7\text{GHz}}{1.8\text{GHz}} = 16.0 \quad (3.7)$$

So, the IF phase noise of a 60GHz subharmonic SIW SOM is predicted as:

$$-85\text{dBc/Hz/100kHz} + 20\log\left(\frac{23}{16}\right) = -82\text{dBc/Hz/100kHz} \quad (3.8)$$

which solely considers the loaded Q of the SIW cavity, while ignoring the phase noise contributed by the active device.



(a) Size of 28GHz SIW cavity

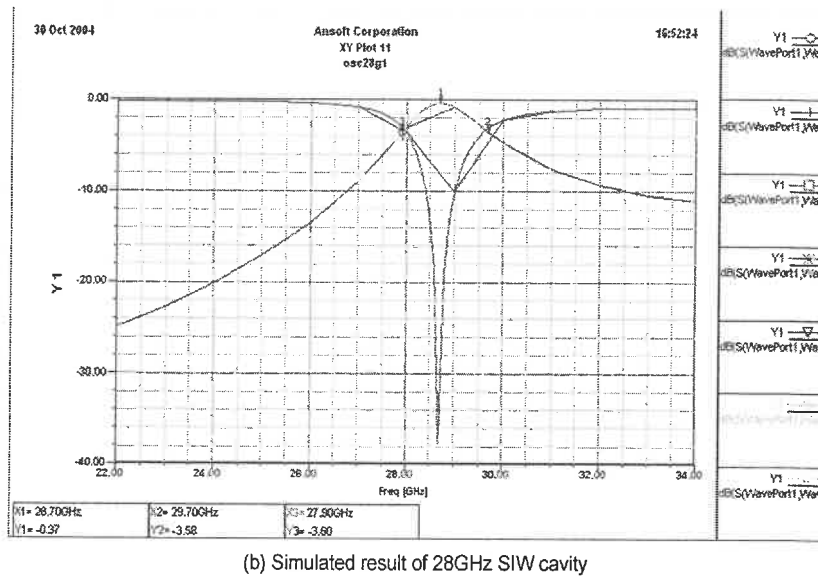


Fig.3.17 Simulated results of a 28GHz SIW cavity

3.6. Electric Performance measurement

Besides the phase noise of mixed signals discussed in the last section, there are other electrical performances that need to be tested and analyzed for the SIW SOM. These include the oscillating frequency drift by the DC variation, the conversion gain and the P_{1dB} gain compression. The phase noise and drift of oscillation frequency are related to the working characteristics of the oscillator. The conversion gain and the P_{1dB} gain compression are the working characteristics of the mixer. As for the SOM, all of these characteristics related to oscillators and mixers need to be discussed.

1. Oscillating frequency drift by the DC variation

The feedback SOM circuits presented in this thesis are designed on small signal S-parameter. So the DC bias has little effect on oscillation frequency. This can be seen in Fig.3.18, which shows the measured LO frequency as a function of DC bias. When $V_{ds} = 1.5V$, V_{gs} is changed from $-0.1V$ to $-0.6V$, the LO frequency shifts from 14.312 GHz to 14.347 GHz with about 35 MHz increasing. As $V_{gs} = -0.6V$, V_{ds} is tuned from 1.25V to 2.0V, the variation of the LO frequency is within 24 MHz, from 14.360-GHz to 14.336 GHz. So variation of DC wouldn't affect the oscillating frequency very much in this design.

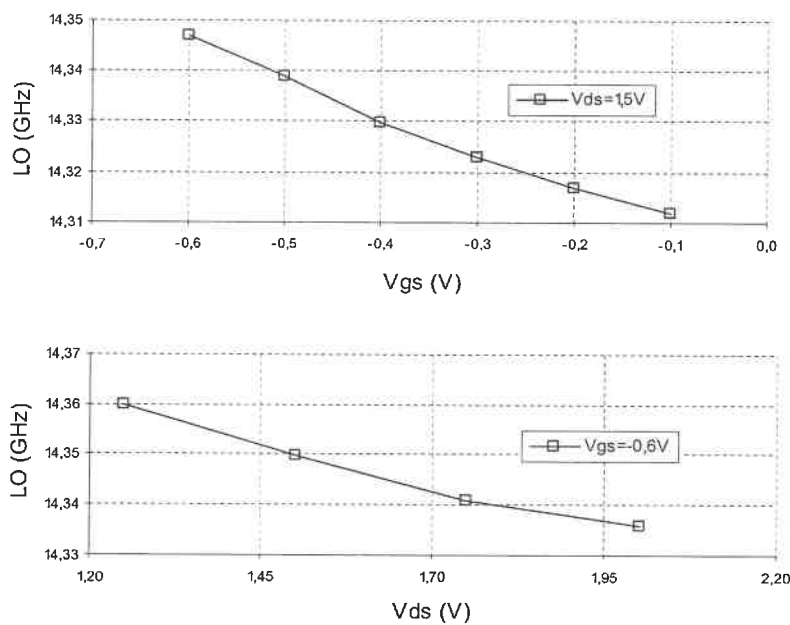


Fig.3.18 Measured oscillating frequencies drift as a function of DC bias

2. Conversion gain measurement

Mixer design focused on the conversion gain optimization, because good conversion efficiency is the most important design criteria for a frequency converter circuit, while the SOM designer will have to think more about how to achieve oscillator and mixer simultaneous by utilizing one active device. Normally, SOM designers optimize the conversion gain by adjusting the DC bias under oscillating condition. The setup to test the conversion gain of SIW SOM includes a WR28 horn antenna (MTC), the SIW SOM circuit, a patch antenna, a signal generator (SMR40), a spectrum analyzer (FSIQ40), a power meter (ML2438A) and a power sensor (MA2474A); the picture of the whole setup is shown in Fig.3.19. First, the horn antenna is set as a transmitter by connecting it to the signal generator, and the receiving power for the isolated patch antenna, which is the same as the antenna integrated with the SIW SOM, is then measured as a reference. Afterward, the SIW SOM circuit is used to replace the isolated antenna. In this case, the transmitted signal is received by the patch antenna in the SIW SOM circuit, and the mixed IF signal power is read from the spectrum analyzer. The difference between the reference power obtained from the patch antenna, and the IF power obtained from the output of the circuit, is the conversion gain of the SIW SOM. The tested data and the calculated conversion loss are noted in table 3.1, and the losses of the cable are taken into account in the calculations.

Table 3.1 Tested data of conversion loss

Transmit Signal Input Power (dBm)	Referenced Receive Power (dBm)	SIW SOM Receive IF Power (dBm)	Conversion Loss (dB)
12	-9.2	-17.8	8.6
11	-10.2	-18.7	8.7
10	-11.1	-19.7	8.6
9	-12.0	-20.6	8.6
8	-12.9	-21.6	8.7
7	-13.9	-22.5	8.6
6	-14.8	-23.4	8.6
5	-15.8	-24.3	8.5
4	-16.7	-25.3	8.6
3	-17.7	-26.2	8.5
2	-18.7	-27.2	8.5
1	-19.7	-28.2	8.5
0	-20.7	-29.2	8.5

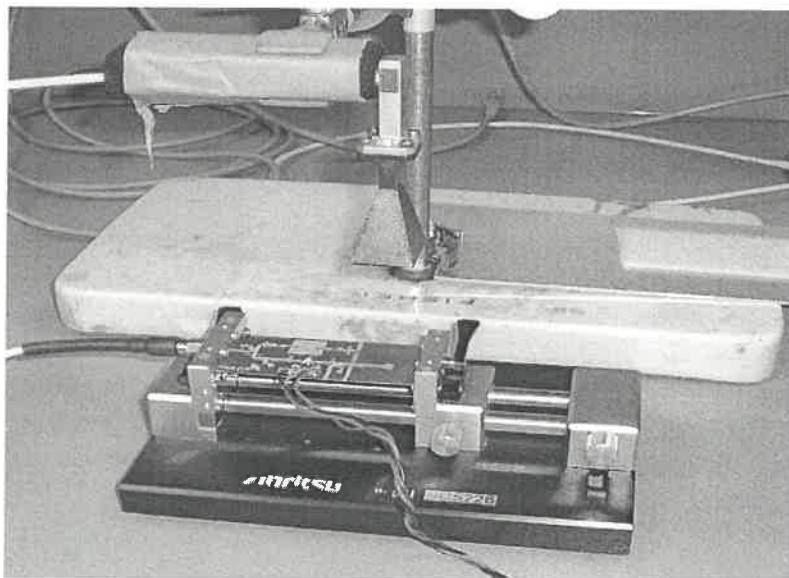
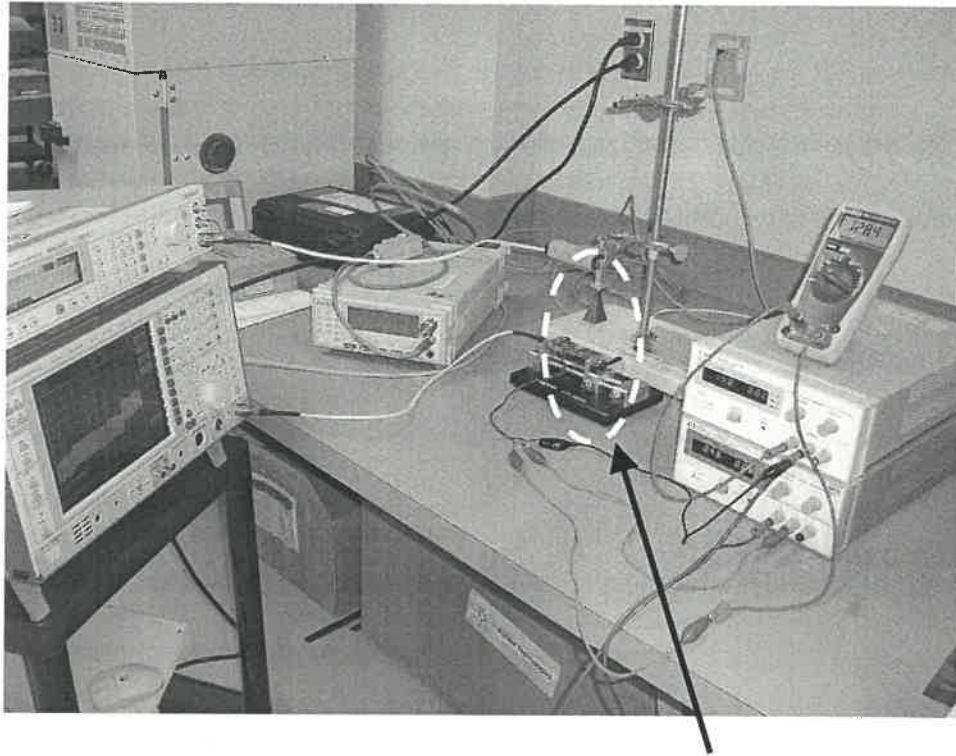


Fig.3.19 Conversion gain test setup of SIW SOM integrated with patch antenna

The sensitivity of the conversion gain to gate and drain bias, with fixed 30.4 GHz RF input frequency, were measured and the tested results are shown in Fig.3.20. As the gate voltage is reduced from -0.1V to -0.6V, the conversion gain keeps on increasing and the best operation is achieved at $V_{gs} = -0.6V$. As the gate voltage is reduced continuously, the AFT36077 works in a voltage below pinch off and consequently no current flows through the drain. With V_{gs} fixed at -0.6V, the drain voltage variation from 1.25V to 2V only makes the conversion gain have a ripple within 1-dB, so the drain voltage doesn't affect the conversion gain very much.

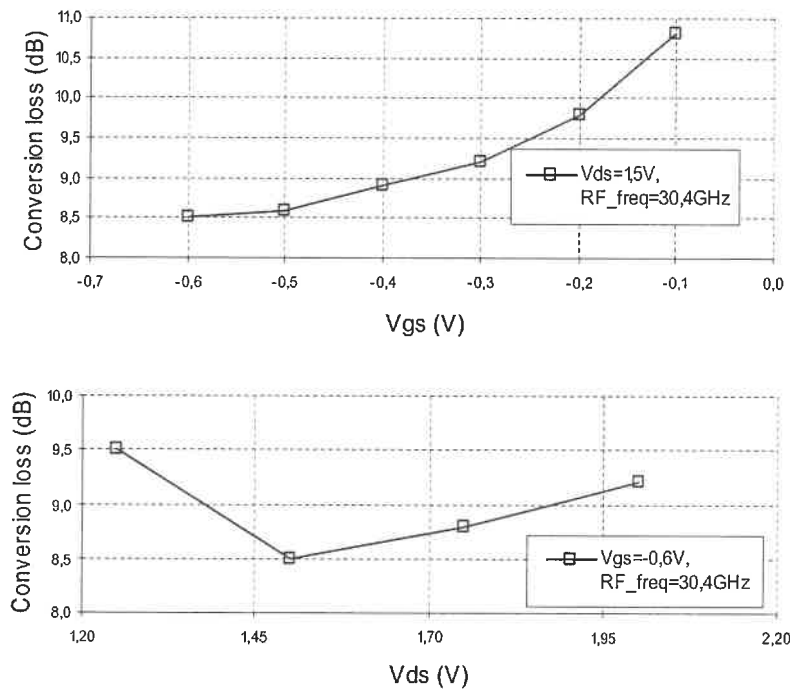


Fig.3.20 Measured conversion loss as a function of the V_{ds} and V_{gs}

3. P_{1dB} gain compression measurement

The P_{1dB} gain compression of SIW SOM is tested by inputting an 18 GHz RF signal from the coupler port, because using conversion gain test set up to measure P_{1dB} gain compression is not efficient as too much power is lost in space transmission. A 3.653-GHz IF signal is obtained by 18 GHz RF frequency mixing with the LO. From the spectrum analyzer, the levels of IF are read as changing the input RF level changes. The curve of the IF power as a function of RF level, shown in Fig.3.21, demonstrates that the output P_{1dB} gain compression of the design is $-9dBm$. Normally, the P_{1dB} gain compression of a SOM is determined by the active device used in the circuit.

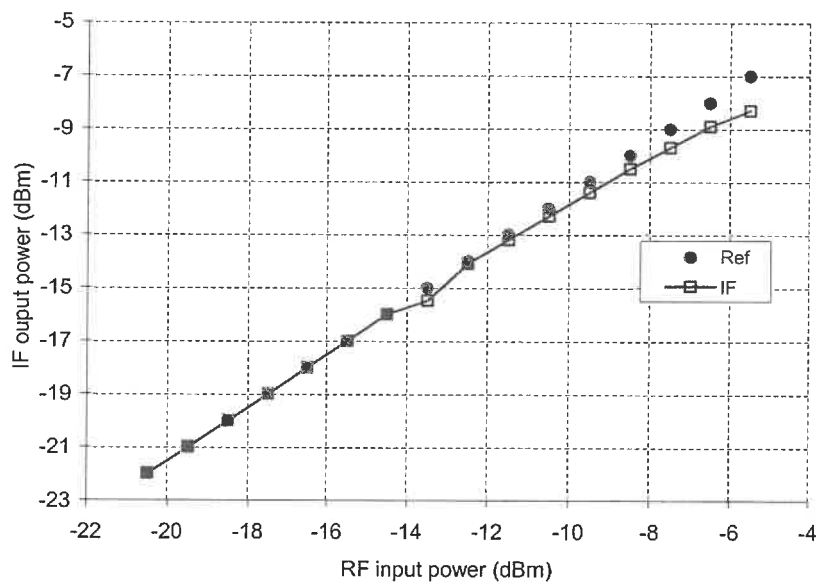


Fig.3.21 P_{1dB} Gain compression measured result

3.7. Summary

In this chapter, the SIW SOM was integrated with a patch antenna. An improved design technique, based on characteristics of the SIW cavity and the feedback SOM working principle, is proposed here. Applying the new technique (connecting FET with SIW cavity directly) means no amplifier design required and no circuit-tuning problems. There is a good agreement between the simulated and measured loop gain & phase responses. The IF phase noise, better than that obtained in Chapter 2, is achieved as $-85\text{dBc/Hz @}100\text{ kHz}$.

Closed loop gain reduced due to port mismatch is analyzed. The IF phase noise of feedback SIW SOM working at higher frequency can be predicted according to Leeson's formula. A 28 GHz SIW cavity is simulated with loaded Q of 16, which will give the IF phase noise as $-82\text{dBc/Hz @}100\text{ kHz}$ when it used in a 60 GHz subharmonic SIW SOM system.

Under lab testing conditions, the working performances are measured for both oscillating and mixing of the subharmonic SIW SOM. The LO frequency pulled by DC variation is very small in this design. The average conversion loss of subharmonic mixing function is 8.6dB, and the optimal conversion loss is achieved at $V_{ds} = 1.5V$, $V_{gs} = -0.6V$. The output $P_{1\text{dB}}$ gain compression related to active device is -9dBm.

CHAPTER 4

SUGGESTIONS FOR FUTURE WORK

SOMs have been widely used in the Doppler radar sensor such as [22], [25] and [23], transponder [24], retrodirective arrays [26] and transceiver in communication system [27]. This section first discusses an up-converter schematic by using SIW SOM. Then a novel front-end structure is proposed for millimetre-wave imaging radar. At the end, a reflect-type SIW SOM topology is demonstrated.

4.1. SIW SOM Applied in an Up-Converter

The design and the experimental measurement for the SIW SOM working as a down-converter have been discussed previously in the thesis. A schematic of it working as an up-converter is illustrated in Fig.4.1. An IF signal is fed at the gate of FET, and a RF signal is generated from the drain. The challenge in such a design is that, at the output, the RF signal is too close to the internal oscillator frequency. For example, if the input IF frequency is 2 GHz, then mixed RF signal is only 2 GHz higher than $2LO$. As a result, a millimeter-wave filter with high Q and good rejection at stop band is necessary in the up-converter design. A quasi-elliptical filter built by the SIW technique is the best choice to achieve a pure spectrum of the output RF signal, because its topology can be manufactured in the same substrate as the other parts of the design.

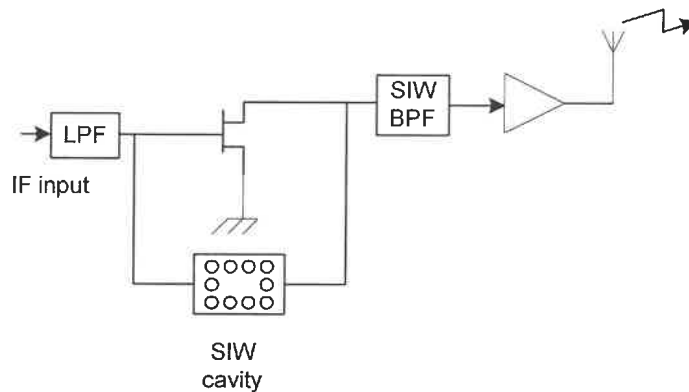


Fig.4.1 Schematic of an SIW SOM up-converter

4.2. SIW SOM Applied in Millimeter-Wave Imaging Radar

The imaging radar refers to systems and techniques for collection and processing radar backscatter data from a planar array. In generally, the system includes antenna, transmitter, receiver, signal and display processing. SAR (Synthetic Aperture Radar) is the side-watch imaging radar widely applied in air navigation; but for aircraft landing, forward-watch imaging radars are required. There are several different architectures of such radars used in aircraft landing and ocean remote sensing systems.

A 95 GHz radar sensor for autonomous landing guidance was presented in [28], which used circularly polarized Cassegrain antenna and multi-pulse, multi-port processing techniques. Another 94 GHz FMCW imaging radar introduced in [29] used a vertical polarized, twist Cassegrain reflector to form a horizontal scan fan beam, with an FMCW signal getting data from vertical direction. FOPAIR (Focused Phased Array Imaging Radar) X-band radar was presented in [30] for ocean remote sensing, which

was a focused-phased array imaging radar by applying a 128 element switched receive array. A 35 GHz pulse radar [31] was constructed by an electro-mechanically scanned antenna, transmitter, MIMIC receiver, and a display processor. These imaging radars belong to active imaging systems.

A passive imaging system is different from an active radar system since it does not transmit any power; it just receives the blackbody radiation from the navigation view. The general construction of a passive imaging system includes three parts, an antenna array, a radiometer and a signal processor. Several different imaging systems were described in [32], such as plasma camera and autonomous aircraft landing system, which employed the focal plane array receivers. Another millimeter-wave focal-plane array camera, presented in [33], had direct detection low noise receivers at W-band. A real time imaging system was presented in [34], which had a frequency-scanned phased array and 32 low noise MMIC receivers working as a pupil plane array.

Chapter 4 indicates that the SIW SOM can work as a low cost receiver integrated with patch antenna. It is possible to design an imaging antenna array with each element including a SIW SOM receiver. The phase controlled array is widely used in beam steering. Since there is no phase-locked oscillator in the SIW SOM that makes a non-coherent phase relationship between each element, it is not easy to design a phase-controlled beam scan array integrated with the SIW SOM. The other electronic scanning technique is beam switching, which is a simple solution through rapid switching among the fixed beams. Beam switching has excellent advantage applying to the SIW SOM, because the switches work in the IF frequency, which creates a very fast, efficient and

low-cost scanning system. A multiple-beam millimeter-wave substrate lens antenna for wireless communication was presented in [35], and that kind of substrate lens antenna is also a good candidate for millimeter-wave imaging radar.

It is possible to use a compact structure to realize a front end with the SIW SOM and a two-dimension substrate lens array which is illustrated in Fig.4.2. A square planar, formed by 60° cutoff of a cylinder, is covered to the patch elements integrated with the SIW SOM circuits. As a result, a fan beam steering with limited scan angle is achieved by that kind of cutoff cylinder lens. In most forward-watch imaging systems, such as aircraft landing, the limited scan angle is enough for the navigation view. Each feed element of the cutoff cylinder lens is a compact receiver constructed by a SIW SOM with integrated patch antenna; and switches are set at the LPF port to realize the beam steering.

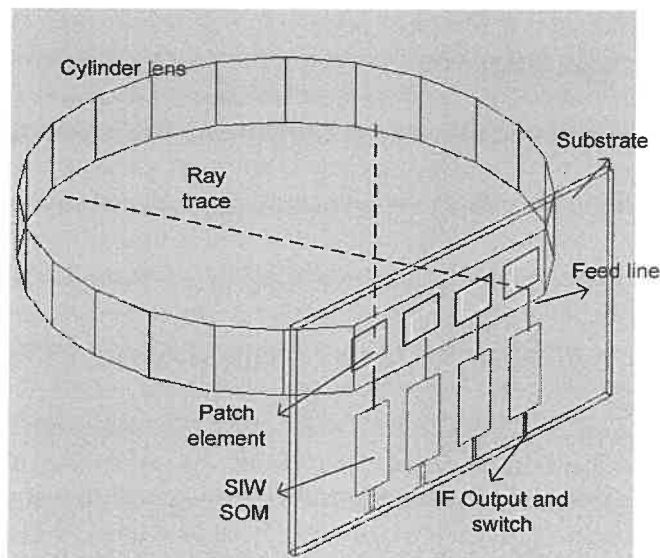


Fig.4.2 Front-end structure of SH SIW SOM integrated with cutoff cylinder lens

Fig.4.3 is simulated results of the beam scan by using HFSS, where the cylinder lens is built by Rexolite ($\epsilon_r = 2.54$), with depth as 200mil and radius as 600mil. Four patch elements are arranged in the cutoff square plane. The scan angle is $\pm 24^\circ$, with beam width as 13° . A narrow beam width will be realized by increasing the radius of the cylinder lens.

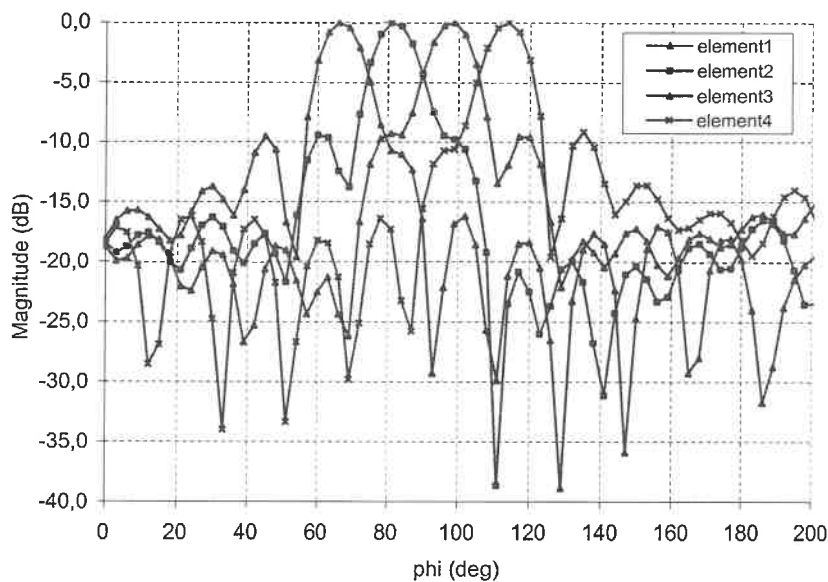


Fig.4.3 Simulated beam scan of cylinder lens fed by four patch elements

Since the fan beam can only scan in one dimension, which is not enough to display two dimension images, one simple solution is proposed. A transmitter scans fan beam in time sequence vertically, while a receiver set orthogonally to the transmitter, receives fan beam data horizontally. The crossing part of the orthogonal beams produces two dimension pixels. The principle of operation is illustrated in Fig.4.3.

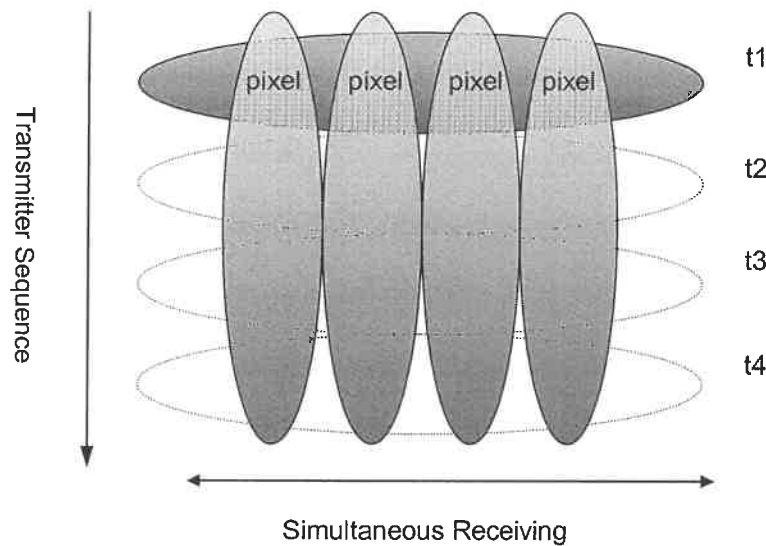


Fig.4.4 The principle of operation of two-dimension imaging construed by fan beam steering

4.3. Reflect-type SIW SOM Structure

In addition to feedback SIW SOM, it is also possible to design reflect-type SIW SOM if a nonlinear model of the active device is available. A reflect-type SIW oscillator designed referred to [36] and its layout is shown in Fig.4.5. Since the ATF36077 model provided in ADS is not accurate, the oscillation doesn't work at the design frequency. If an accurate model of the FET can be built, this prototype design should work well. Because the reflect-type SIW SOM design bases on large signal model, the conversion gain will be better than feedback SIW SOM, while the phase noise performance should be analyzed again.

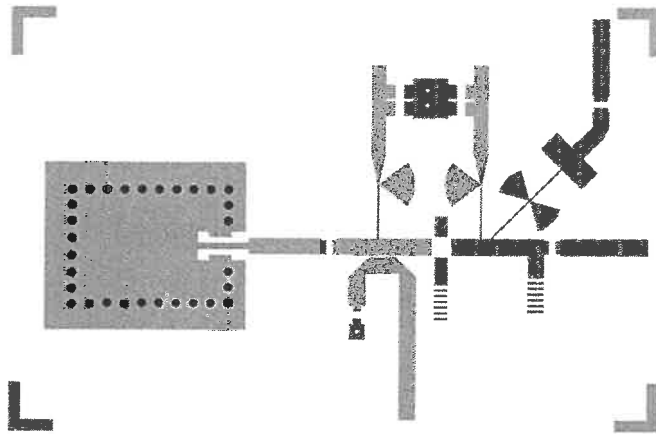


Fig.4.5 Layout of a reflect-type SIW SOM

CONCLUSIONS

The objective of the thesis was to apply the SIW technique in a millimetre-wave self-oscillating mixer design. A nonlinear model of the transistor is unavailable, so a feedback SOM schematic is chosen, and its working concept is simulated with ADS. A TRL calibration technique is used to measure the small signal S-parameters of the FET, and a 14 GHz amplifier is designed based on the measured results. A conventional SOM, with paralleled CML as feedback loop, is designed, and then an SIW SOM, by using the SIW cavity as resonant, is presented. The IF phase noise comparison between the two designs indicates that the SIW SOM provides a phase noise with 10 dB to 20 dB less than that of the conventional SOM.

An improved design of the feedback SIW SOM is developed. A 30GHz subharmonic SIW SOM integrated with the patch antenna is then designed. An improved IF phase noise of $-85\text{dBc/Hz}@100\text{kHz}$ was achieved. The gain reduction by the port mismatch in this design is discussed. Leeson' formula is used to demonstrate the relationship between the loaded Q of a SIW cavity and the phase noise of an SIW SOM. A 28GHz SIW cavity is simulated to predict that a 60GHz subharmonic SIW SOM can get IF with $-82\text{dBc/Hz}@100\text{kHz}$ phase noise. Performances of the subharmonic SIW SOM with integrated patch antenna are tested. The variation of DC bias give oscillator frequency shift in several dozen MHz/mV effect; the conversion loss of subharmonic SIW SOM is around 8.6dB and the optimal DC bias is found to achieve the best conversion loss; the output P_{1dB} gain compression is measured at -9dBm .

Because of the presence of the SIW cavity, a measured 15dB IF phase noise improvement is obtained by comparing the result in [25], where a 34GHz SOM was constructed with a distribution LC resonator. A measured 8.6dB conversion loss is comparable with the result presented in [11].

Finally the thesis introduces the application of the SIW SOM. A novel front-end structure for millimeter-wave imaging radar is proposed by utilizing SIW SOM and two-dimension substrate lens. The beam scan of the lens fed by four patch elements is simulated. An up-converter structure of the SIW SOM and a reflect-type SOM are suggested for the future research.

The original contribution of this work is:

1. Analysis and comparison of the phase noise of SIW SOM with other SOM structure.
2. Development a simplified technique to design the feedback SIW SOM.
3. Design, implementation and test of a 30GHz subharmonic SIW SOM with integrated patch antenna.
4. Proposal a number of application by utilizing SIW SOM.

REFERENCES

- [1] Y. Tajima, "GaAs FET applications for injection oscillators and self-oscillating Mixers," *IEEE Trans. on MTT.*, Vol. 27, pp.629-632, July 1979.
- [2] G. Gonzalez, "Microwave transistor amplifiers: analysis and design ," *Prentice-Hall, Inc.*, 1997
- [3] M. Sironen, Y. Qian and T. Itoh, "A sbharmonic self-oscillating mixer with integrated antenna for 60-GHz wireless application," *IEEE Trans. on MTT.*, Vol. 49, pp.442-450, March 2001.
- [4] N. Bourhill, S. Iezekiel and D.P. Steenson, "A balanced self-oscillating mixer," *IEEE Microwave and guide wave letters*, Vol. 10, pp. 481-483, Nov. 2000.
- [5] M. J. Roberts, S. Iezekiel, and C. M. Snowden, "A compact subharmonically pumped MMIC self-oscillating mixer for 77 GHz application," *IEEE MTT-S*, Vol. 3, pp.1435-1438, June 1998.
- [6] J. Zhang, Y. Wang and Z. Chen, "Integration of a self-oscillating mixer and an active antenna," *IEEE Microwave and Guided wave letters*, Vol. 9, pp. 117-119, March 1999.
- [7] R.W. Rhea, "Oscillator design and computer simulation," Chapter 2, chapter3, *McGraw-Hill*, 1997.
- [8] B. Meskoob and S. Prasad, "Loop-gain measurement and feedback oscillator design," *IEEE Microwave and guide wave letters*, Vol. 2, pp. 375-377, September 2000.
- [9] Y. Cassivi and K. Wu, "Low cost microwave oscillator using substrate integrated waveguide cavity," *IEEE Microwave and guide wave letters*, Vol. 13, pp. 48-50, February 2003.
- [10] I. Kipnis andA. S. Khanna, "Large-Signal computer-aided analysis and design of Silicon Bipolar MMIC Oscillators and Self-Oscillating mixers," *IEEE MTT-s*, Vol.37, pp.558-564, March 1989.

- [11] T. Huang and S. Chung, "A new balanced self-oscillating mixer (SOM) with integrated antenna," *IEEE Antenna and Propagation Sym.*, Vol.1, pp89-91, June 2003.
- [12] G. Wang, T. Li, W. Liu and S. Yang, "A low cost DBS low noise block downconverter with a DR stabilized MESFET self-oscillating mixer," *IEEE MTT-S*, Vol.3, pp.1447-1450, May 1994.
- [13] Y. Cassivi, L. Perregrini, K. Wu and G. Conciauro, "Low-cost and high-Q millimeter-wave resonator using substrate integrated waveguide technique", *Eur. Microwave Conf.*, Milano, Italy, 2002.
- [14] D.M. Pozar, "Microwave Engineering," Chapter 6 pp.313-317, *New York, Toronto, Wiley*, 1998.
- [15] J. Papapolymerou, J. Cheng, J. East and L.P.B. Katehi, "A Micromachined High_Q X-band Resonator," *IEEE Microwave and guide wave letters*, Vol. 7, No.6, pp.168-170, June 1997.
- [16] ADS, version 2003A, Agilent Inc.
- [17] *IEEE Standard Dictionary of Electrical & Electronics Terms*, 2nd ed., New York, NY: IEEE Inc. 1977, pp. 27.
- [18] J. Q. Howell, "Microstrip Antenna", *IEEE Trans. Antennas Propag.*, Vol.AP-23, No.1, pp.90-93, Jan. 1975.
- [19] J. Zurcher and F. E. Gardiol, "Broadband Patch Antenna", chapter 9 pp.177-188, Artech House Inc, 1995.
- [20] D. H. Evans, "A millimeter-wave self-oscillating mixer using a GaAs FET harmonic-mode oscillator", *IEEE MTT-S Int. Microwave Symp. Dig.*, 1986, pp. 601-604.
- [21] D. B. Leeson, "A simple model of feedback oscillator noise spectrum", *Proceedings of the IEEE*, pp.329-330, Feb. 1966.
- [22] B. M. Armstrong, R. Brown, E. J. Duffin and J.A.C. Stewart, "Short range Doppler radar sensor using a baritt diode", *IEEE MTT-S*, Vol. 80, pp.501-503, May 1980.

- [23] C. Tsironis, "12GHz receiver with self-oscillating dual-gate MESFET mixer", *Electr. Letter*, 20th, Vol.17, No. 17, August 1981.
- [24] K. Cha, S. Kawasaki and T. Itoh, "Transponder using self-oscillator mixer and active antenna", *IEEE MTT-S*, Vol. 1, pp.425-428, May 1994.
- [25] J. L. Caceres and J.Perez, "A single MESFET downconverter for TVRO application", *IEEE MTT-S*, Vol. 2, pp.777-780, May 1998.
- [26] D. M. K. Ah Yo, W. E. Forsyth and W. A. Shiroma, "A 360° retrodirective self-oscillating mixer array", *IEEE MTT-S*, Vol. 2, pp.813-816, June 2000.
- [27] C. M. Montiel, Ph.D. thesis, Univ. of Texas A&M, 1997.
- [28] K. L. Koester and W. Vaillancourt, "Talons 95 GHz radar sensor for autonomous landing guidance", *IEEE Aerospace and Electronic Systems Magazine*, Vol.7, pp.40-44, July 1992.
- [29] L. Q. Bui, D. Uecker, E. Loose and Y. Alon, "Test results of an experimental autonomous aircraft landing system utilizing a 94 GHz FM-CW imaging radar", *IEEE MTT-S*, Vol.2, pp.857-860, June 1993.
- [30] R. E. McIntosh, S. J. Frasier and J. B. Mead, "FOPAIR: a focused array imaging radar for ocean remote sensing", *IEEE Trans., Geoscience and Remote Sensing*, Vol.33, pp.115-124, Jan. 1995.
- [31] F. Sadjadi, M. Helgeson, M. Radke and G. Stein, "Radar synthetic vision system for adverse weather aircraft landing", *IEEE Trans., Aerospace and Electronic Systems*, Vol.35, pp.2-14, Jan. 1999.
- [32] P. F. Goldsmith, C.-T. Hsieh and G. R. Huguenin, "Focal plane imaging system for millimeter wavelengths", *IEEE Trans. MTT*, Vol.41, pp.1664-1657, Oct. 1993.
- [33] M. Shoucri, R. Davidheiser, B. Hauss, P. Lee, M. Mussetto, S. Young, and L. Yujiri, "A passive millimeter wave camera for aircraft landing in low visibility conditions", *IEEE Aerospace and Electronic Systems Magazine*, Vol.10, pp.37-42, May 1995.

- [34] C. Martin, J. Lovgerg, S. Clark and J. Galliano, "Real time passive millimeter-wave imaging from a helicopter platform", *Digital Avionics Systems Conferences, Proc.* Vol.1, pp.2B1/1 - 2B1/8, Oct. 2000.
- [35] X. Wu, G.V. Eleftheriades and T. E. van Deventer-Perkins, "Design and characterization of single- and multiple-beam mm-wave circularly polarized substrate lens antennas for wireless communications", *IEEE Trans. MTT*, Vol.29, pp.431-441, March 2001.
- [36] Y. Kwon, C. Cheon, N. Kim, C. Kim, I. Song and C. Song, "A Ka-band MMIC oscillator stabilized with a micromachined cavity ", *IEEE Microwave and guide wave letters*, Vol. 9, pp. 360-362, Sept. 1999.

ÉCOLE POLYTECHNIQUE DE MONTRÉAL



3 9334 00314299 7